UAB
Universitat Autònoma de Barcelona

Modelling Nanomagnetic Systems: Towards the Skyrmionic Bit

Josep Castell Queralt

Universitat Autònoma de Barcelona
Departament de Física

Modelling Nanomagnetic Systems: Towards the Skyrmionic Bit

Josep Castell Queralt

Under the supervision and tutoring of:

Carles Navau Ros

Nuria Del Valle Benedí

Submitted in part fulfilment of the requirements
for the degree of Doctor of Philosophy in Applied Physics
of the Universitat Autònoma de Barcelona, March 2023

Abstract

This thesis is devoted to the theoretical modeling of skyrmionic devices, with a focus on optimizing the transport of skyrmions under realistic conditions without compromising simulation performance. Three different theoretical frameworks are used: the first two are the well-known micromagnetic model and the Thiele equation, and the third one is the Fokker-Planck equation of a skyrmion that is developed in this thesis. The main contributions of this thesis are: (i) a new set of numerical meshes that can optimize micromagnetic simulations in some scenarios, (ii) the design of the skyrmionic rails, a skyrmionic device that speeds-up skyrmions by an order of magnitude, (iii) the development of a deterministic, yet probabilistic, approach to model the dynamics of skyrmions at room temperature that outperforms the other theoretical models, and (iv) the incorporation of the granularity to the above approach without significantly increasing the computational cost of the simulations, resulting in a model that offers the best realism/performance ratio of all the current methods in the literature, to the best of our knowledge. The methodology introduced in this thesis represents a step forward in modeling skyrmions under realistic conditions since it is efficient, yet simple enough, to be spread throughout the community.

Author's Note

After dedicating the last 4 years to scientific research and listening to various opinions, I have decided to write my thesis as a compendium of articles. While I understand the many advantages of a traditional thesis, such as the ability to explain research in more detail, the learning process for the Ph.D. student, and the potential for sharing knowledge, I believe that the scientific community (and society at large) is moving towards a world where we are inundated with information. With approximately two million scientific articles published every year, staying up-to-date with the latest research is becoming increasingly challenging, and doctoral theses, once a vital means of transmitting information, are losing their relevance.

Due to the global pandemic, I suffered many delays in my research, and last year I found myself with two half-finished projects (Papers C and D). I had to decide whether I wanted to write a classical thesis with the risk of leaving these two research projects unfinished, or write two more papers and do a thesis in compendium format. I decided to do the latter because I believe that well-written papers could have more impact on the scientific community than a classical thesis; in my opinion, the classical format is becoming obsolete in this massive publishing system that the scientific community is following. Due to its format, this thesis is divided into two parts: the introduction intended to provide the context and theoretical background necessary for a better understanding and assessment of the second part, four articles referred to as Papers A, B, C, and D, where the main results of my research are presented and discussed. However, I do not recommend a linear reading of this document and kindly ask you to follow the instructions below.

The introduction, is divided into four chapters: a general background introduction to spintronics and skyrmions, the second and third chapters are devoted to the micromagnetic and the rigid model, respectively, and it finishes with the conclusions and final remarks. Papers A and B are embedded in chapter 2, while Papers C and D are embedded in chapter 3. Chapters 2 and 3 are structured as follows. First, a theoretical framework is introduced and the different elements needed for the calculations done in the Papers are introduced. This is followed by an introductory subsection for each paper, in which the main results are presented, contextualized, and discussed. I strongly recommend reading each Paper after its corresponding introductory subsection before continuing the lecture of the rest of the thesis. To be more precise (look at the table of contents you can find on page v), I recommend reading Paper A after section 2.5.1, Paper B after 2.5.2, Paper C after 3.4.1, and Paper D after 3.4.2.

I also would like to highlight that besides obtaining all the scientific results shown in this thesis, during my PhD I devoted a great portion of my time to develop a software package writen from scratch to both, perform numerical simulations and analize the obtained data. We have used this package to do all the simulations done in this thesis and the corresponding papers. We hope that we can soon share this package with the scientific community.

I - INTRODUCTION

Contents

Chapter 1

Motivation and Background

In a few centuries historians will probably refer to our era as the Information or Digital age. Claude Shannon, with his paper "A Mathematical Theory of Communication",[1] laid the cornerstone for the Digital Revolution. During the 1950s research institutions, the military, and businesses developed the first computer systems to automate mathematical calculations and improve telecommunications. But it was during the 1970s that the digital revolution flooded people's daily lives with the proliferation of personal computers. Yet there is already much more than just personal computers.

Digital data records (like DVDs, flash memories, or hard drives), the internet, smartphones... In the last few decades, mankind has experienced the most significant technological leap in history. And it has not stopped. 5G, artificial intelligence and much more applications are coming.[2–4] Even so, for all these new technologies to flourish, the scientific community has to overcome two significant hurdles.

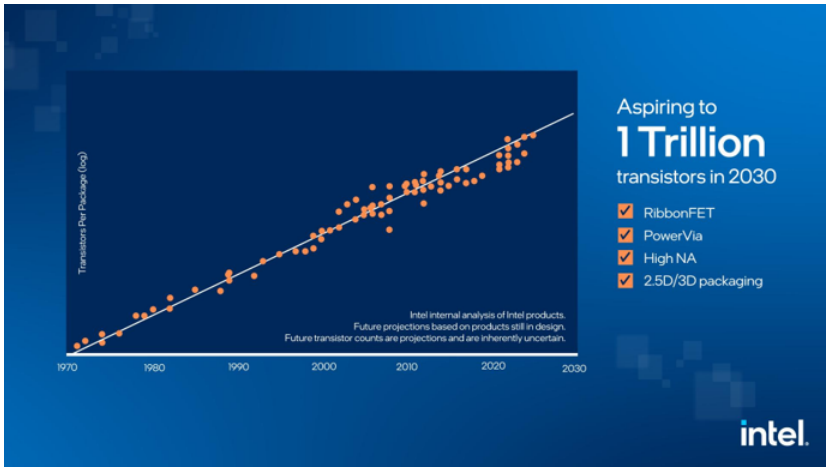

Figure 1.1: Scheme of Intel's processors power and the year they were produced. We can see the linear trend that approximately follows Moore's law. Published by Intel in Ref. [5]

The first one, is the physical limitations of Moore's law,[6,7] Fig. 1.1, imposed by heating and the Heisenberg uncertainty principle. In 1965, Gordon Moore, co-founder of the well-known company Intel, predicted that the number of transistors on a chip would approximately double every two years without a significant increase in cost. During the late 1900s, the strategy to achieve that was to make the transistors smaller and smaller. Recently, we reached a transistor size small enough to sense quantum effects in electrical circuits. The industry has found other

strategies to further increase transistor density such as more efficient packaging or the recent explosion of GPUs. However, all these strategies will reach their limit in the following years.

The second major obstacle is the energy consumption, Fig. 1.2. This huge technological jump came with a cost. Nowadays people are much more aware of climate change and we are trying to become a greener and more sustainable society. Still, most people are not conscious of the growing environmental impact of digital technologies. For example, every time we do a Google search we are emitting 0.2 g of CO_2.[8] Moreover, if the information techonology (IT) sector was a country, it would be the third largest energy consumer in the world.

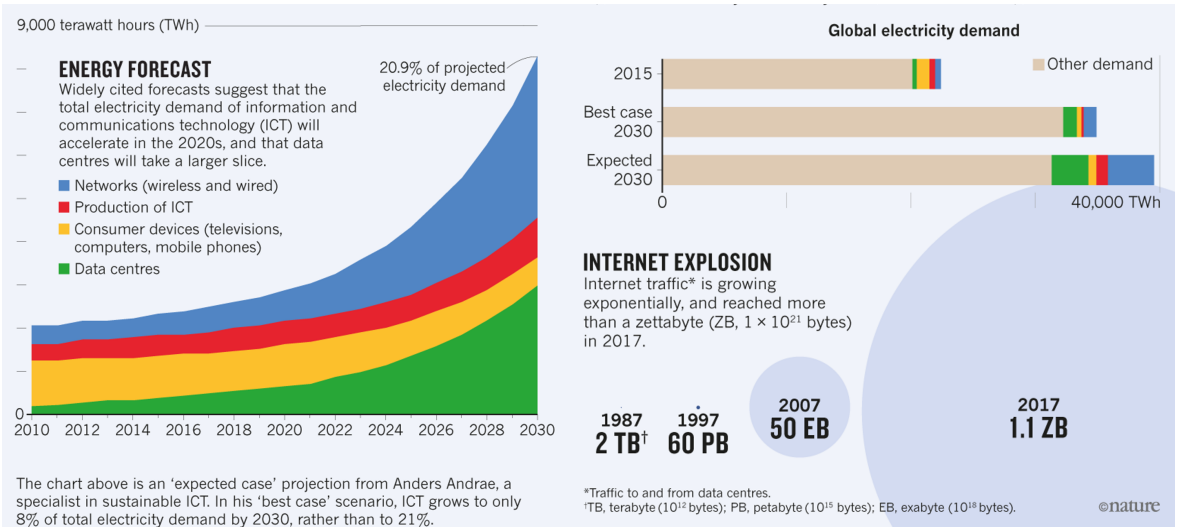

Figure 1.2: Figure from Ref. [8]. In the left side we can see the evolution of the energy consumption until 2017 and a forecast up to 2030. On the upper right side we can see the evolution of the energy consumed by the IT sector compared with the other sectors. In the bottom right side the exponentially growing internet traffic is displayed in a scheme.

More powerful and energy-efficient devices are essential to ensure the steady growth of our digital developments without compromising the environment. This need motivated the emergence of spin electronics, or spintronics.[9,10] The field of spintronics pretends to build solid-state devices that are based on the flow of electrons and their spin. Indeed, while electronic devices only take advantage of the electron's electric charge, spintronics pretends to build devices that exploit both the electrical charge and the spin of the electrons. In addition to the plethora of physical phenomena that can be exploited, pure magnonic spin currents, in contrast to electrical currents, do not produce heat by Joule effect.[11] By overcoming one of the main limitations of conventional electronic devices, spintronics has the potential to significantly enhance the power and energy efficiency of these devices.

Spintronics emerged thanks to a series of scientific advances that took place between the 60s and 90s,[9,12–15] among which the following stands out the discovery of giant magnetoresistance independently by Albert Fert [14] and Peter Grünberg [15] in 1988. Thanks to this discovery they were awarded the Nobel Prize in 2007. The number of possible applications and proposed devices escalated quickly,[9,16–18] being the spin transfer torque magnetoresistive random access memory (STT-MRAM) and the racetrack memory the more promising applications, Fig. 1.3. Nowadays spintronics is not only relevant in the field of classical computation and information processing but is also of great interest in the fields of quantum[19] and neuromorphic[20,21] computing.

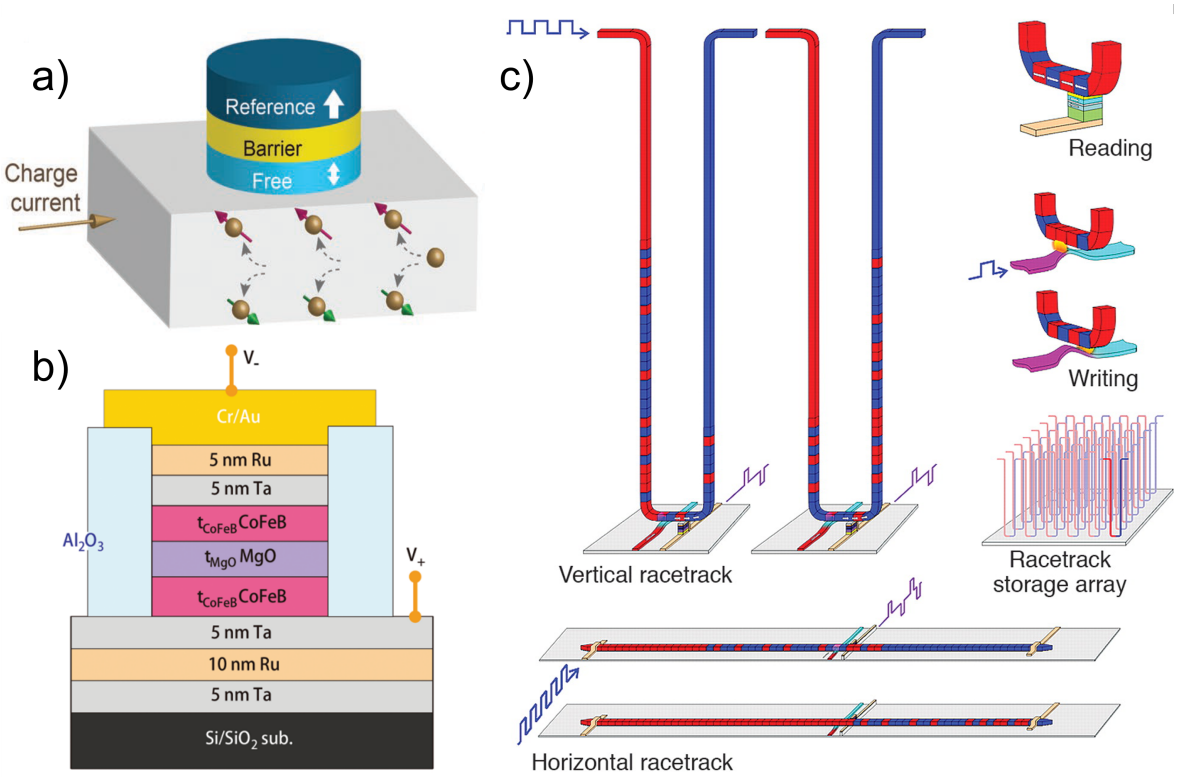

Figure 1.3: a) Figure from Ref. [22]. Scheme of the simplest design of a MRAM. Its design is based on the dependence of the magnetoresistance of the system as a function of the orientation of the magnetization of the free layer. b) Figure from Ref. [22]. Scheme of a modern design of a MRAM. c) Figure from Ref. [18]. Sketch of the domain wall racetrack memory proposed by Parkin, and its functioning. The magnetic orientation of the domain wall would be a 1 or a 0. The domain walls would be moved with spin currents, thus it is a solid state drive (it does not require the motion of internal elements).

1.1 Skyrmions and state of the art

Thanks to a large number of advances in spintronics and material science,[23] in 2010 was experimentally detected for the first time the existence of a magnetic structure that would open a new path in spintronics: the skyrmion.[24,25] Skyrmions were proposed by Tony Skyrme in the 1960s in the field of particle physics.[26] They were topologically protected particles, in the sense that no continuous deformation of the field configuration could destroy them. The same theoretical model was used in other fields like Bose-Einstein condensates,[27] liquid crystals,[28] or quantum Hall systems.[29,30] But the field in which skyrmions would achieve their maximum impact would be in the field of the helimagnetic systems, where the skyrmions are spin textures with particle-like behavior.[31]

Hence, in the field of magnetism, skyrmions are magnetic whirling structures that can be found on certain magnetic materials,[32] Fig. 1.4. They were theoretically predicted in the 1990s[33] and experimentally found in 2010,[24,25] but the interest in this structure skyrocketed after they were proposed for a new kind of racetrack memory by Albert Fert [34] in 2013. After that, skyrmions have been envisioned as the building blocks of a new generation of memories and spintronic devices thanks to their outstanding properties.[31,34–38]

Skyrmions are very small magnetic structures, their size range from a few tens of nanometers

at temperature $T = 0$ K to 100-200 nm at room temperature (RT).[39,40] Skyrmions have a very robust metastability thanks to their topological protection.[41] They have been found at RT experimentally[42] and it has been theoretically proved that their lifetime is long enough to be used as information carriers.[41] Finally, skyrmions can be moved with relatively small electrical currents (compared with other magnetic structures, such as domain walls) through the torques generated by the interaction between the spins of the material and the spins of a free spin current.[34,43]

Skyrmions are usually found in materials where the Dzyaloshinskii–Moriya interaction is present.[44–49] This interaction occurs when there is a lack of inversion symmetry in the crystallographic structure of the material and it can appear in two kinds of materials: bulk materials or ultrathin films through the interaction between the interfaces, which is known as interfacial Dzyaloshinskii–Moriya interaction (iDMI). In this thesis, we will only work with ultrathin systems so we will only refer to two-dimensional systems from now on. It has been also stated that "skyrmions" can be stabilized through the classical magnetic field in more common magnetic systems. However, these magnetic structures are much larger (micrometer) than the regular skyrmions and they are usually referred to as magnetic bubbles.[50]

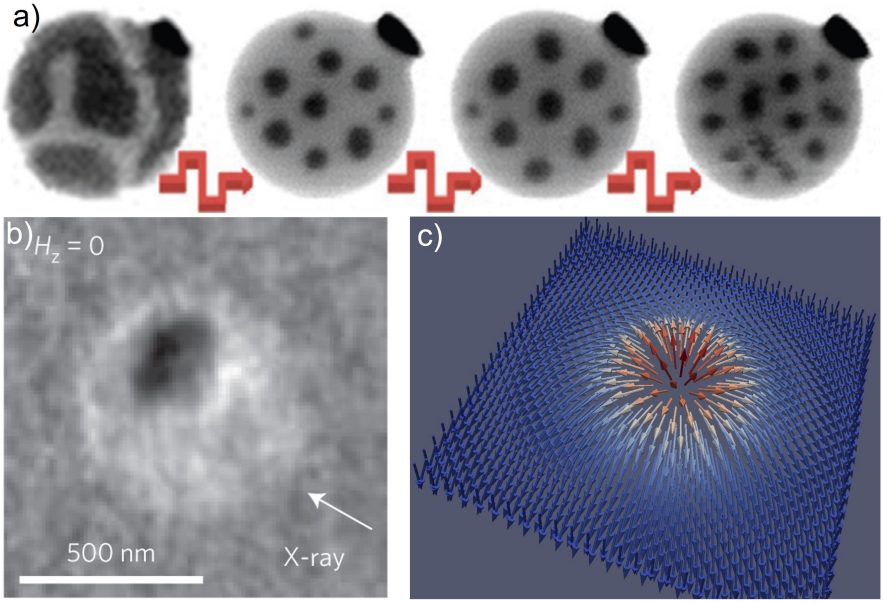

Figure 1.4: a) Figure from [42]. Experimental observation of skyrmions at room temperature with magnetic transmission soft X-ray microscopy. b) Figure from [46]. Experimental observation of a skyrmion at room temperature at the ALBA synchrotron. c) Scheme of the spin texture of a Néel skyrmion, the kind of skyrmions that is stabilized by interfacial Dzyaloshinskii–Moriya interaction and that will be studied in this thesis.

Three processes need to be studied and optimized if skyrmionic devices are to become a reality.[31,32,51] If they are supposed to be bits of information, we should first of all be able to nucleate/annihilate them individually, which is equivalent to writing/erasing data. Next, we will want to transport them as fast and efficiently as possible. And finally, we will want to "operate" with them, which will depend on the type of application we are talking about.

From the theoretical point of view, these processes have been studied in depth at low temperature (LT) mainly with two theoretical models: the micromagnetic model[52,53] (MM)

and the rigid model.[54] The micromagnetic model studies the magnetization dynamics at the sub-micrometer length scale. To do so, the discrete atomic magnetic moments distribution is approximated by a continuous magnetization distribution. The rigid model assumes that the skyrmion is a rigid magnetization distribution that moves through space, behaving like a particle. The rigid model provides the skyrmion trajectory. This model is derived from the MM and it is much simpler, but it cannot simulate phenomena where the skyrmion is deformed or destroyed and may be inaccurate in some scenarios. The MM has been used to simulate the nucleation/annihilation of skyrmions.[55–68] Both models have been used to study the skyrmionic transport by improving the original design of the skyrmion racetrack memory[43,69–80] or with the design of alternative skyrmion-transport devices.[81–83] Also, the interaction between the skyrmions with external agents (different than the edges of the material), like defects or non-homogeneities in the material,[84–99] granularity,[100–110] voltage-controlled magnetic anisotropies (VCMAs),[111–116] other skyrmions,[117] notches,[118] magnetic field gradients,[63,119–121] temperature gradients,[122–124] or superconductors[125] have been studied. Based on these advances, some skyrmionic applications have already been designed, such us logic gates.[126–129]

However, at RT the advances made are not so abundant[58,105,130–136] and many important issues remain elusive. That is because skyrmionic dynamics at RT are stochastic since a Brownian-like motion arises. This phenomenon hugely increases the complexity of the analytical models and the computational power required for the simulations. However, we expect spintronic devices to work at RT, so it is essential to make physical simulations as realistic as possible. Moreover, very promising applications that take advantatge of the stochatistic properties of skyrmionic dynamics to generate random numbers have been proposed.[135,137,138]

In this thesis, we have contributed with our grain of sand to these three essential processes (nucleation/annihilation, transport, and applications) with special emphasis to the transport stage. First, most of the studies of the nucleation/annihilation of skyrmions have been done in confined geometries. We detected some inconsistencies in the results of micromagnetic simulations in axisymmetric systems. In Paper A, we prove that some of these results have a questionable validity and we provide two new numerical meshes that solve this problem and outperform the commonly used quadrilateral mesh.

Second, in the transport stage, we developed an alternative to the skyrmionic racetrack memory, and we provided a new theoretical model to study skyrmionic dynamics at RT: in Paper B we introduce the skyrmionic rails, two linear defects engineeried in a way that speed up the skyrmions by an order of magnitude while compressing and guiding them, outperforming the classical racetrack memory; in Paper C, we developed a deterministic model to study the skyrmionic dynamics at non-zero temperatures, that incorporates all the complexity of the Brownian motion with high performance; and in Paper D, we used this model to study the viability of the racetrack memory in real conditions (RT and granularity). Furthermore, Paper C and Paper D also contribute at the third stage, the development of applications. We present a methodology that allows to theoretically model possible skyrmionic devices (like the random number generators[135,137]) in real conditions that consists in solving a simple partial differential equation (PDE), which could be done with many popular commercial softwares.

Chapter 2

Micromagnetism

Historically, when studying magnetic systems, and magnetic materials in particular, classical electromagnetism was used. However, as technology and physics progressed and smaller systems became more relevant, Maxwell's equations fell apart. When approaching the nanometric scale the atomic structure becomes rellevant, quantum effects arise, and classical physics no longer works. Hence, to study magnetic materials at the nanometric scale we would have to solve an unmanageable amount of coupled Schrödinger equatios.

Micromagnetics[52,53] is the framework that studies magnetic systems at submicrometer length scales: large enough to ignore the internal structure of the material, yet small enough to resolve magnetic structures such as skyrmions.[139] This semiclassical theory was developed to bridge the gap between classical magnetism and the quantum mechanical treatment of exchange interactions as first described by Heisenberg.

In the semiclassical atomic model, we assume that each atom has a single localized classic magnetic moment, $\boldsymbol{\mu}$, which is the average of the quantum magnetic moments of the nucleons and electrons that constitute the atom. If we have a large number of atoms and they form a ferromagnetic (FM) system, we can assume that the spatial variation of $\boldsymbol{\mu}$ is smooth. Therefore, we can construct a continuous magnitude for the magnetic moment, $\boldsymbol{\mu} \to \mathbf{M}(\mathbf{r})$,[52] where $\mathbf{r}$ is the positon. This magnetization field, $\mathbf{M}(\mathbf{r})$, becomes a semiclassical version of the classical-electromagnetism magnetization. For example, it generates the same stray field predicted by Ampêre's law, but its time dynamics takes into account quantum-mechanical effects. In addition to the continuous limit, in the original MM another approximation is done: we assume that we are at temperature $T = 0$, or, at least, far from the Curie temperature, T_C. Hence, we can assume that the magnetization has a constant modulus M_s, the saturation magnetization. Then, $\mathbf{M}(\mathbf{r}, t) = M_s\mathbf{m}(\mathbf{r}, t)$, where t is the time, and $\mathbf{m}(\mathbf{r}, t)$ is a unitary vector. The step from the discrete $\boldsymbol{\mu}$ to the continuous $M_s\mathbf{m}(\mathbf{r}, t)$ is called the micromagnetic approximation and is sketched in Fig. 2.1

2.1 The Landau-Lifshitz-Gilbert equation

So far, one might wonder what are the differences between the MM and classical magnetism. The first main difference is that inside the ferromagnet we have an effective field, $\mathbf{H}_{\text{eff}}$. This effective field contains the classical magnetic field generated by $\mathbf{M}$ and the externally applied magnetic field, but also includes extra terms coming from the quantum-mechanical interactions between the magnetic moments of the material. The second difference is that the time evolution of $\mathbf{M}$ is given by the Landau-Lifshitz-Gilbert (LLG) equation. The LLG equation is a PDE describing the precessional motion of $\mathbf{M}$ around an effective field $\mathbf{H}_{\text{eff}}$ at each point.[140–142] It is an equation of empirical origin and it is written as

$$(1+\alpha^2)\frac{\mathrm{d}\mathbf{M}}{\mathrm{d}t} = -\gamma\mathbf{M}\times\mathbf{H}_{\text{eff}} - \frac{\gamma\alpha}{M_s}\mathbf{M}\times(\mathbf{M}\times\mathbf{H}_{\text{eff}}) + \boldsymbol{\tau}, \tag{2.1}$$

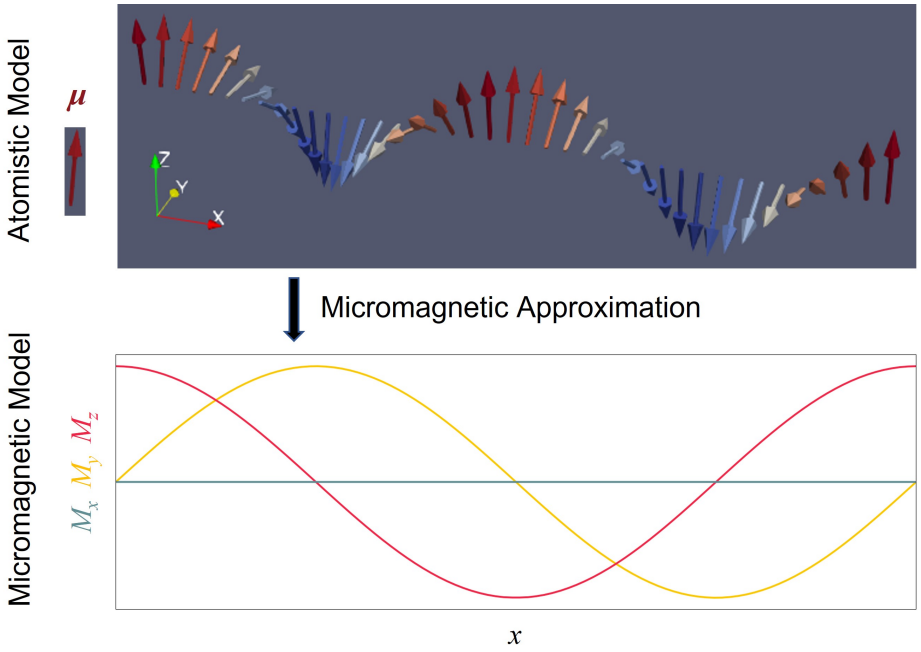

Figure 2.1: Scheme to represent the micromagnetic approximation. The top figure is a discrete distribution of atomistic magnetic moments. They form an helicoide. The MM approximation is displayed at the bottom figure, where the discrete atomistic moments, $\boldsymbol{\mu}$, are approximated by the continuos vectorial field $\mathbf{M}$. All the physical magnitudes are in arbitrary units.

where, α is the dimensionless Gilbert damping constant, γ is the gyromagnetic constant ($\gamma = 2.21 \cdot 10^5$ m A^{-1} s^{-1}), and $\boldsymbol{\tau}$ contains the external torques, generated by external spins, for example, a spin current flowing through the ferromagnet. Since $\mathbf{M}$ has a fixed modulus, its dynamics are constrained to rotations, so the terms of the LLG equation are torques acting on the magnetization. $-\gamma\mathbf{M} \times \mathbf{H}_{\text{eff}}$ is the precession torque and empirically represents the Larmor precession on the micromagnetic scale. If a single magnetic moment was set in the void and an external magnetic field was applied, $\mathbf{M}$ would precess around the applied field, Fig. 2.2, pink arrow. However, FM materials are solid state systems, and when $\mathbf{M}$ precess around $\mathbf{H}_{\text{eff}}$ it is damped. This is accounted by the term $-\frac{\gamma\alpha}{M_s}\mathbf{M} \times (\mathbf{M} \times \mathbf{H}_{\text{eff}})$. As the precession is damped, $\mathbf{M}$ moves toward the direction of minimum energy, which is being parallel with $\mathbf{H}_{\text{eff}}$, Fig. 2.2, yellow arrow.

To solve Eq. (2.1) we need to calculate $\mathbf{H}_{\text{eff}}$, $\boldsymbol{\tau}$, and the boundary conditions (BC) which are highly system dependent. In all the papers presented in this thesis we focus on 2D skyrmionic systems, which are ultrathin FM films (located at the plane $z = 0$) with a heavy-metal (HM) substrate or multilayers with alternating FM films and heavy-metals.[48,49]

2.2 Effective field

In classical electromagnetism the magnetic field $\mathbf{H}$ is generated by variations of the electrical field, free currents, and magnetic poles. None of these explain or justify the existence of the FM phase. The reason is that the FM phase exists because of interactions of quantum origin such as the exchange interaction.

In the MM, these quantum-mechanical effects can be incorporated by transforming the hamiltonians of these interactions into effective fields using the micromagnetic approximation.[52,53]

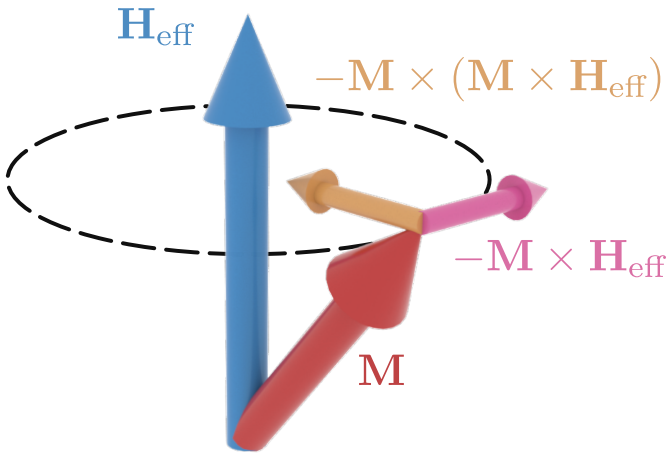

Figure 2.2: Schematical representation of the torques that $\mathbf{M}$ would experiment when is subjected to the effects of an $\mathbf{H}_{\text{eff}}$, and the trajectory that it would follow.

To do so, first we write the discrete Hamiltonian of the interaction, $\mathcal{H}(\boldsymbol{\mu})$. Then, by performing the continuous limit[†], it is transformed into a continuous energy density $\epsilon(\mathbf{M})$. Then, from the magnetic energy expression we obtain the corresponding effective field, $\mathbf{H}_{\text{eff}}(\mathbf{M})$:

$$\epsilon = -\frac{1}{2}\mu_0 \mathbf{M} \cdot \mathbf{H}_{\text{eff}}, \quad \rightarrow \quad \mathbf{H}_{\text{eff}} = -\frac{1}{\mu_0}\frac{\delta \epsilon}{\delta \mathbf{M}}, \tag{2.2}$$

where μ_0 is the vacuum permeability, and δ indicates functional derivative. In the systems studied in this thesis, the following interactions are considered: exchange, uniaxial magnetocrystalline anisotropy, and interfacial Dzyaloshinskii–Moriya. Therefore, the total Hamiltonian (not accounting for external interactions), $\mathcal{H}$, of our system is

$$\mathcal{H} = \mathcal{H}_{\text{ex}} + \mathcal{H}_{\text{an}} + \mathcal{H}_{\text{DM}}. \tag{2.3}$$

$\mathcal{H}_{\text{ex}}$ is the Hamiltonian of the exchange interaction, $\mathcal{H}_{\text{an}}$ is the Hamiltonian of the uniaxial anisotropy interaction, and $\mathcal{H}_{\text{DM}}$ is the Hamiltonian of the iDMI. The classical demagnetizing field it is renormalized within the uniaxial anisotropy. It has been shown that in 2D systems this is a valid approximation.[97,143,144] The main reason is that despite the long range of the interaction, in 2D systems the shape of the field is almost the same than the anisotropy field, so the demagnetizing and the uniaxial magnetic fields are almost proporcional. Then the demagnetizing field is taken into account renormalizing the anisotropy constant, K. Thermal effects can also be incorporated into the MM as an effective field. This is not done here since thermal effects are not considered in papers A and B but will be discussed in the following chapter.

Exchange interaction

This interaction comes from a quantum mechanical effect, discovered independently, by physicists Werner Heisenberg and Paul Dirac in 1926. This interaction favors the alignment of neighboring magnetic moments to the same direction.[52,145,146] As a simplified picture, when two fermions are identical, due to the Pauli exclusion principle, they can not have the same wave function so they can not be in the same place if they have the same spin state. Then, the electrons with the spin pointing to the same direction are more spaced between

[†]The detailed step-by-step continuous limit for each interaction is done in Ref. [52].

them, and since these fermions repel each other (have the same electrical charge), when they are spaced, the electrostatic energy becomes smaller, and the energy of the system is lowered. The Hamiltonian of this interaction can be written as

$$\mathcal{H}_{\text{ex}} = -J \sum_{<i,j>} \boldsymbol{\mu}_i \cdot \boldsymbol{\mu}_j, \tag{2.4}$$

where J is the exchange integral, and we sum over all the pairs of neighboring magnetic moments $\boldsymbol{\mu}_i$. After doing the micromagnetic approximation, we obtain the exchange interaction energy density, ϵ_{ex}:

$$\epsilon_{\text{ex}} = \frac{A}{M_s^2}\left[(\nabla M_x)^2 + (\nabla M_y)^2 + (\nabla M_z)^2\right], \tag{2.5}$$

where A is the exchange interaction constant, which depends on J, $|\boldsymbol{\mu}|$, and the lattice parameter of the material. M_ν ($\nu = x, y, z$) are the components of $\mathbf{M}$. Eq. (2.5) can be written as:

$$\epsilon_{\text{ex}} = -\frac{A}{M_s^2}\mathbf{M} \cdot \boldsymbol{\nabla}^{\mathbf{2}}\mathbf{M}, \tag{2.6}$$

from which the exchange field, $\mathbf{H}_{\text{eff}}^{\text{ex}}$, can be obtained directly from Eq. (2.2):

$$\mathbf{H}_{\text{eff}}^{\text{ex}} = \frac{2A}{\mu_0 M_s^2}\boldsymbol{\nabla}^{\mathbf{2}}\mathbf{M}. \tag{2.7}$$

Uniaxial anisotropy

A FM material is said to have magnetocrystalline anisotropy if it is energetically easier to magnetize along certain directions than others,[52,147] or in other words, if it has an easy axis. This occurs as a consequence of the interaction between the crystal's magnetic moments with the crystal's electric field, so it depends on the particular crystal structure. In this thesis, we only consider systems with uniaxial anisotropy with the easy axis perpendicular to the ultrathin film ($\hat{\mathbf{z}}$ direction). The Hamiltonian of this interaction can be written as,

$$\mathcal{H}_{\text{an}} = -\kappa \sum_i (\boldsymbol{\mu}_i \cdot \hat{\mathbf{z}})^2, \tag{2.8}$$

where κ is the anisotropy parameter and depends on the material. Therefore, the magnetic moments will tend to align along the z-axis (no preference between up or down). Now, we proceed as before: the micromagnetic approximation is done, replacing $\boldsymbol{\mu}_i$ for a vectorial field $\mathbf{M}(\mathbf{r})$ and we rewrite Eq. (2.8) as an energy density:

$$\epsilon_{\text{an}} = -\frac{K}{M_s^2} M_z^2, \tag{2.9}$$

where K is the effective anisotropy constant (recall that a correction has been added to account for the classical demagnetizing field) which depends on κ, $|\boldsymbol{\mu}|$, and the lattice parameter of the material. From ϵ_{an}, the effective field coming from the anisotropy, $\mathbf{H}_{\text{eff}}^{\text{an}}$, is calculated:

$$\mathbf{H}_{\text{eff}}^{\text{an}} = \frac{2K}{\mu_0 M_s^2} M_z \hat{\mathbf{z}}. \tag{2.10}$$

Interfacial Dzyaloshinskii-Moriya interaction

The iDMI is only present in some systems, and it enables the metastability of Neél Skyrmions,[44–49] Fig. 1.4. It is an indirect exchange interaction that arises from the strong spin-orbit coupling

between two magnetic moments of the FM film with a third one of the HM substrate, Fig. 2.3. This interaction favors that the neighboring spins are oriented perpendicularly. The Hamiltonian of this interaction is:

$$\mathcal{H}_{\mathrm{DM}} = \sum_{<i,j>} \mathbf{D}_{ij} \cdot (\boldsymbol{\mu}_i \times \boldsymbol{\mu}_j), \tag{2.11}$$

where $\mathbf{D}_{ij}$ depends on the position of the three atoms, Fig. 2.3, being always perpendicular to their plane, and the summation is done over all the pairs of neighboring magnetic moments. If we use the micromagnetic approximation, we can rewrite the Hamiltonian as an energy density:

$$\epsilon_{\mathrm{DM}} = -\frac{D_{\mathrm{DM}}}{M_s^2}\mathbf{M} \cdot \left[(\nabla \mathbf{M})\,\hat{z} - \nabla M_z\right], \tag{2.12}$$

where D_{DM} is the iDMI parameter which depends on $\mathbf{D}_{ij}$, $|\boldsymbol{\mu}|$ and the lattice of the material. From ϵ_{DM} we compute the corresponding effective field:

$$H_{\mathrm{eff}}^{\mathrm{DM}} = \frac{2D_{\mathrm{DM}}}{\mu_0 M_s^2}\left[(\nabla \mathbf{M})\,\hat{z} - \nabla M_z\right]. \tag{2.13}$$

This energy interaction is minimized when $(\boldsymbol{\mu}_i \times \boldsymbol{mu}_j)$ is antiparallel to $\mathbf{D}_{ij}$, and the directions of the two magnetic moments form an angle of $\pi/2$.

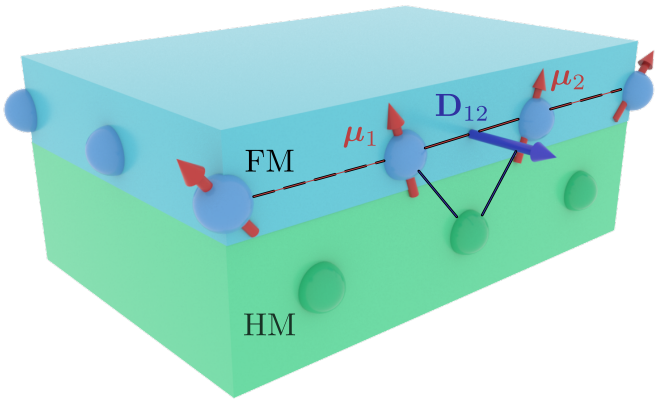

Figure 2.3: Sketch the iDMI. Two atoms of the ultrathin FM film (blue) are interacting between them through a third atom located in the HM substrate (green). Figure from [34].

Hence, while the anisotropy favors the alignment of the spins in the z-axis (perpendicular to the film), the exchange favors that all the magnetic moments point in the same direction (have the most uniform distribution possible). Therefore, if we only had these two interactions, the most stable configuration would be to have all the magnetic moments pointing in the z-axis direction, but the iDMI favors a relative tilt between neighboring magnetic moments of $\pi/2$. The trade-off between these interactions could favor a smooth spin canting which makes Néel skyrmions metastable.

Applied Field

To all the previous internal energetic interactions of the material we have to add the externally applied field, $\mathbf{H}_{\mathrm{ap}}$ to have the total $\mathbf{H}_{\mathrm{eff}}$. Hence, the energetic term coming from this interaction is,

$$\epsilon_{\mathrm{Z}} = -\mu_0 \mathbf{M} \cdot \mathbf{H}_{\mathrm{ap}}. \tag{2.14}$$

Notice that this energy term does not have the $\frac{1}{2}$ term. This is because it is an external interaction. So, finally, we can write the total energy density of our system, ϵ_{m}, and the total effective field, $\mathbf{H}_{\mathrm{eff}}$, summing all the terms:

$$\epsilon_{\mathrm{m}} = -\frac{A}{M_s^2}\mathbf{M}\cdot\nabla^2\mathbf{M} - \frac{K}{M_s^2}M_z^2 - \frac{D_{\mathrm{DM}}}{M_s^2}\mathbf{M}\cdot[(\nabla\mathbf{M})\,\hat{z} - \nabla M_z] - \mu_0\mathbf{M}\cdot\mathbf{H}_{\mathrm{ap}}, \tag{2.15}$$

$$\mathbf{H}_{\mathrm{eff}} = \frac{2A}{\mu_0 M_s^2}\nabla^2\mathbf{M} + \frac{2K}{\mu_0 M_s^2}M_z\hat{\mathbf{z}} + \frac{2D_{\mathrm{DM}}}{\mu_0 M_s^2}[(\nabla\mathbf{M})\,\hat{z} - \nabla M_z] + \mathbf{H}_{\mathrm{ap}}. \tag{2.16}$$

2.3 External Torques

Two kinds of torques appear in the LLG equation, Eq. (2.1). The first two terms in the right side of the equation depend on $\mathbf{H}_{\mathrm{eff}}$ which depends on $\mathbf{M}$, so they are the torques produced on the magnetization by the magnetization itself (and the applied magnetic fields). However, we can influence the magnetization dynamics by using external torques, the last term in Eq. (2.1). There are several ways in which one can generate torques acting over the magnetization. They mainly focus on generating a spin current flowing through the FM film. In this thesis, we focus on the external torques used to move skyrmions in ultrathin films, the spin transfer torque (STT), and the spin Hall effect (SHE) torque. The STT is the torque generated by the direct injection of a spin polarized current into the FM layer of the system. The SHE torque is the torque generated by the spin current that difusses into the FM layer when a regular electrical current flows through the HM layer.

Spin Transfer Torque

In ordinary currents, formed by electrons with spin $\mathbf{s}$, the average spin polarization $<\mathbf{s}>=0$, so the net interaction between the current and the magnetic moments of the material is 0. However, if a current with $<\mathbf{s}>\neq 0$ is generated, which is called a spin-polarized current, an interaction appears, Fig. 2.4. In Ref. [148] it was computed which would be the torque that an electrical spin-polarized current would produce to $\mathbf{M}$ using quantum mechanical theory.

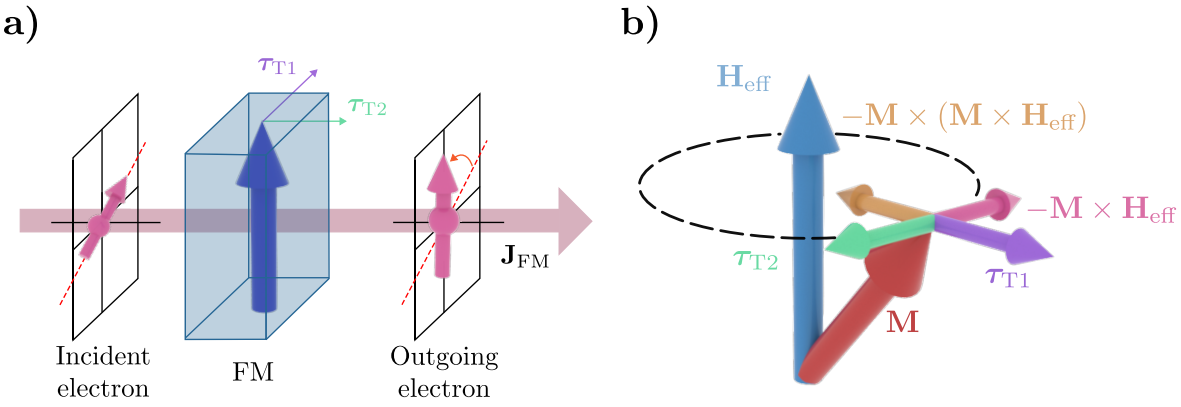

Figure 2.4: Sketch of the the spin transfer torque. a) the electrons (pink arrows) flow through the magnetization of the material (blue arrow), transfering their mangnetic moment producing a torque. b) Equivalent of Fig. 2.2 when the STT is added.

If current flows through our film with $<\mathbf{s}>=(0,0,s)$, two torques appear,[87,148–151] $\boldsymbol{\tau}_{\mathrm{T1}}$ and $\boldsymbol{\tau}_{\mathrm{T2}}$:

$$\boldsymbol{\tau}_{\mathrm{T1}} = -(1+\alpha\beta)(\mathbf{v}_F\cdot\nabla)\mathbf{M}, \tag{2.17}$$

$$\boldsymbol{\tau}_{\mathrm{T2}} = \frac{\beta - \alpha}{M_s}[\mathbf{M} \times [(\mathbf{v}_F \cdot \nabla)\mathbf{M}]], \tag{2.18}$$

where β is called the ratio of nonadiabaticity of spin transfer, a dimensionless parameter that depends on the material and how the current is injected, and $\mathbf{v}_F$ is the effective speed of the spin carriers fed into the FM film, which is proportional to the current density, $\mathbf{J}_{\mathrm{FM}}$.

Spin Hall Effect Torque

Early theoretical designs of skyrmionic devices proposed to move the skyrmions with STT.[34] However, experimentalists soon exposed the drawbacks of this method: ultrathin FM films (0.6-1 nm) are hardly conductors when in-plane currents are applied. Therefore, the heating produced by the currents needed to induce the STT would be critical.

Fortunately, there is a more recent method to move magnetic structures: inducing spin currents through the spin Hall effect.[152–154] This technique consists in making the electrical current flow through the much thicker HM substrate. Then, by spin Hall effect, a spin current diffuses into the FM film, Fig. 2.5. This spin (non-electrical) current produces two torques, $\boldsymbol{\tau}_{\mathrm{H1}}$ and $\boldsymbol{\tau}_{\mathrm{H2}}$, on $\mathbf{M}$, given by,[153]

$$\boldsymbol{\tau}_{\mathrm{H1}} = -\frac{\mu_B \theta_H J_H}{|e| M_s^2 d}\mathbf{M} \times [\mathbf{M} \times \hat{\boldsymbol{\sigma}}], \tag{2.19}$$

$$\boldsymbol{\tau}_{\mathrm{H2}} = -\zeta\frac{\mu_B \theta_H J_H}{|e| M_s^2 d}\mathbf{M} \times \hat{\boldsymbol{\sigma}}, \tag{2.20}$$

where μ_B is the Bohr magneton, J_H the modulus of the electrical current density fed into the HM, $\mathbf{J}_H$, e the electrical charge of the electron, d the thickness of the FM film, $\hat{\boldsymbol{\sigma}}$ the direction of the polarization of the spin-polarized electrons flowing into the ferromagnet, θ_H the spin Hall angle factor, which represents the ratio of the electronic current density circulating through the heavy metal to the polarized spin current density diffusing through the ferromagnet, and ζ is a dimensionless parameter indicating the strength of $\boldsymbol{\tau}_{\mathrm{H2}}$ with respect to $\boldsymbol{\tau}_{\mathrm{H1}}$. In all simulations in this thesis, $\boldsymbol{\tau}_{\mathrm{H2}}$ is neglected (as done usually in the literature) because ζ is usually very small.

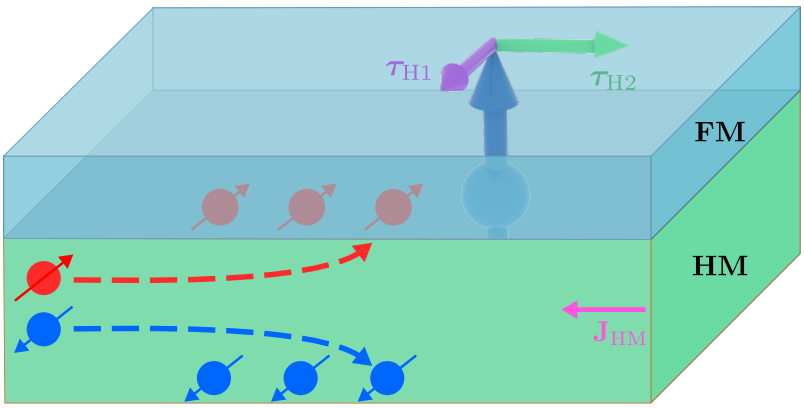

Figure 2.5: Sketch of how the SHE torque is generated. An ordinary electrical current flows through the HM substrate (green). Due to spin Hall effect a spin polarized current that difuses into the FM film is generated. The torques generated are shown.

This technique, in contrast with STT, allows skyrmions to reach velocities on the order of 100

m/s experimentally,[137] as predicted theoretically. Therefore, all the papers in this thesis that deal with skyrmion dynamics (B, C, and D) use SHE torque to drive skyrmions. Also, there are other techniques to induce external torques which are relevant in the field of spintronics, but since they are not used to move magnetic structures they have not been included in this thesis.

2.4 Boundary conditions

With $\mathbf{H}_{\text{eff}}$ and $\boldsymbol{\tau}$ determined, one might think that we have all the necessary ingredients to solve the LLG equation, Eq. (2.1). However, we are dealing with coupled PDEs, so we need BC. The BC used in Papers A and B are introduced here.

Periodic system: Periodic Boundary conditions

When we want to simulate a periodic system, we use periodic boundary conditions (PBC). These boundary conditions are also used to simulate an infinite material when the calculation window is large enough. For example, infinite tracks of magnetic structures use this boundary conditions in the boundaries perpendicular to the track. In paper B, PBC are used. Its mathematical expression is,

$$\mathbf{M}(\mathbf{r}) = \mathbf{M}(\mathbf{r} + \mathbf{r}_T), \tag{2.21}$$

where $\mathbf{r}_T$ indicates the direction in which the system is periodic and $|\mathbf{r}_T|$ is the spatial period.

Edges of the material: Von Neumann boundary conditions

When we want to simulate a finite material, with a real edge, the Dzyaloshinskii-Moriya condition is used. This boundary condition can be found from a variational approach, by minimizing the energy density Eq. (2.15) in a region in the presence of an edge. If we minimize this energy density, we obtain that $\mathbf{M}$ on the edge must fulfill the following condition:[155]

$$\left.\frac{\mathrm{d}\mathbf{M}}{\mathrm{d}\hat{\mathbf{n}}}\right|_{\hat{n}} = \frac{D_{\text{DM}}}{\sqrt{2A\mu_0 M_s^2}} (\hat{\mathbf{z}} \times \hat{\mathbf{n}}) \times \mathbf{M}, \tag{2.22}$$

where $\hat{\mathbf{n}}$ is the vector normal to the edge. The finding of this boundary condition was one of the cornerstones of the theoretical designs of the skyrmionic racetrack. However, this BC induces some problems that we address in Paper A.

Now, all the ingredients are ready to solve the LLG equation in our system, but slightly different conditions have been considered in Paper A and B. In Paper A we solved Eq. (2.1) with an applied field, in a finite geometry, so we used the BC given by Eq. (2.22) but no external torques are considered. In Paper B there is no external fields but we move the skyrmions using SHE torque in an infinite sample, so PBC are used.

2.5 Papers

In this thesis, two papers focus on the micromagnetic framework. Paper A presents the cylindrical mesh (CM), and the radial mesh (RM), two meshes that present higher performance than the usual quadrilateral mesh (QM) when some conditions are met, Fig. 2.6 and 2.7. Paper B presents skyrmionic rails, Fig. 2.8, which consist of two linear defects that, with the optimal properties, can speed up the skyrmions by an order of magnitude while channeling them along predefined paths, and reducing their size.

Paper A is the only one in this thesis that does not address skyrmion dynamics. We undertook the elaboration of this paper when we realized that, in some conditions, micromagnetic simulations could yield unrealistic magnetic structures. These magnetic structures could seem as valid results, but, in Paper A, it is shown that they are the result of numerical errors that are pretty hard to detect and could be overlooked. Despite this topic was a bit far from our original objective of optimizing skyrmionic transport, we could not leave a problem unresolved.

2.5.1 Paper A

MM is an essential tool for theoretical physicists studying magnetic systems at submicrometer length. It consists in solving Eq. (2.1). However, Eq. (2.1) is a vectorial PDE, highly nonlinear, which has no analytical solution (except in some extremely simple cases, e.g., considering a single magnetic moment[52]). Therefore, it is solved numerically. Although in most fields of physics numerical simulations are done using finite elements, MM is an exception. For some technical reasons in terms of performance, when computing the magnetic fields, finite differences are preferred.[156]

The usual approach to solving Eq. (2.1), and the method used by the most popular software, is an explicit method based on a quadrilateral mesh that is integrated over time using a method from the Runge-Kutta (RK) family.[156,157] This approach has proven to be valid but may have its limitations in some specific scenarios.

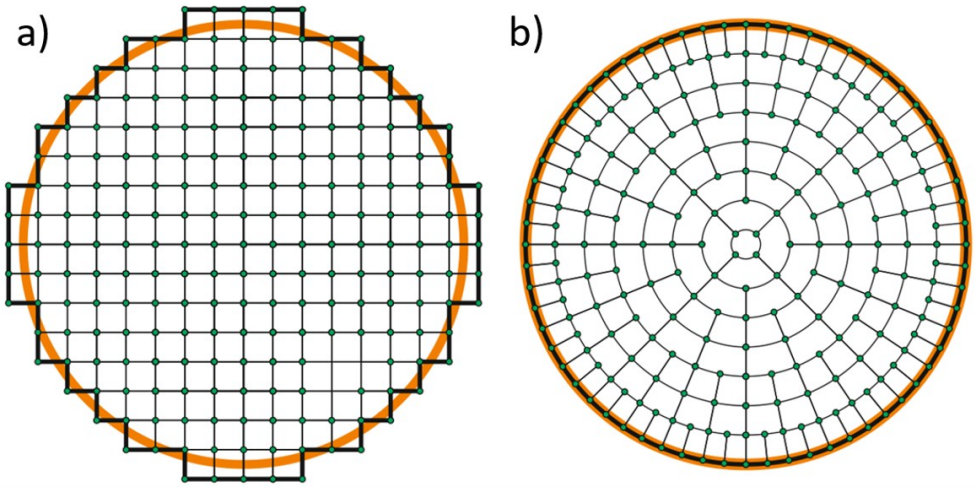

Figure 2.6: Sketch of a circular FM dot (orange circle) meshed with two different meshes. a) The commonly used QM. b) The CM proposed in Paper A.

In the simulation of skyrmionic circular systems, structures similar to Fig. 2.7 have been reported. These structures share the same 90/180° rotational symmetry as the QM and, more importantly, break the cylindrical symmetry of the system, which should be preserved.

In Paper A we show that these are numerically artificial structures, mainly because of two factors. First, skyrmionic BC, Eq. (2.22) are more numerically stressful than the regular ones ($D_{\mathrm{DM}} = 0$). Second, it is shown that the error generated by numerical integration has the same symmetry as the QM. This error distribution is responsible for symmetry breaking.

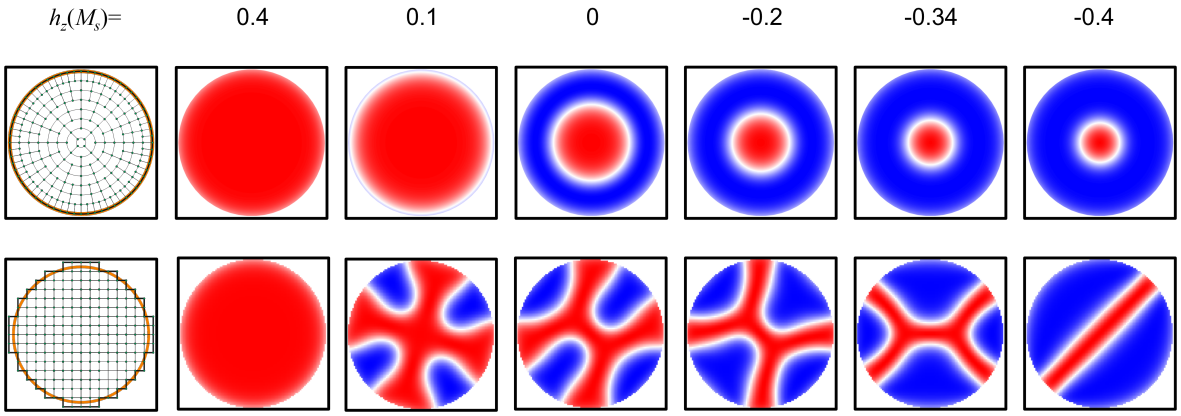

Figure 2.7: Comparison of the same MM simulation done with the CM (top row) and the QM (bottom row). Huge discrepancies are found. In Paper A it is shown the the right results are the ones obtained with the CM and explains the origin of the structures obtained with the QM.

To solve this problem the CM is presented, Fig. 2.6, a mesh that has the same symmetry as the system geometry and therefore does not break the symmetry. The most relevant result is that the same results are obtained with a relatively coarse CM as with a much finer QM. Meanwhile, a coarser QM leads to artificial magnetic structures. Also, the RM is introduced, a mesh that reduces computational time by orders of magnitude when the geometry, applied fields, and initial state are all radially symmetric.

From the results and methods presented in Paper A, it is concluded that for cylindrically symmetric systems the CM (and the RM when possible) is much better in terms of numerical performance. However, the QM can still be used in many cases, but care must be taken with the mesh size.

2.5.2 Paper B

If skyrmions are conceived as bits of information, their fast and energy-efficient transport is a key factor for future spintronic devices. Skyrmions are usually driven by SHE torques, as this is the most efficient technique at the moment.[43,137] In a certain range of current density, known as the linear regime, there is an almost linear dependence between the applied density current, $\mathbf{J}_H$, and the skyrmion velocity.

For lower currents, we enter in the crippling regime. The granularity of the samples, which can be considered a set of pining sites cripples the motion of the skyrmion, making it much more stochastic and even stopping it. The skyrmion is in crippling regime when its velocity is below 15-20 m/s.[101,102,105,158–160] For higher $\mathbf{J}_H$ the skyrmion deforms and may be unstabilized (generating stripes or domain walls) or annihilated. The skyrmion is usually unstablized when its velocity is higher than 200-300 m/s.[43] There is another limitation to the skyrmion motion, the skyrmion Hall effect (SkyHE). The skyrmion does not travel completely perpendicular to the current, it has a relative angle between the perpendicular of the spin current and the resulting velocity, which is known as the skyrmion hall angle.[34,71,87,92,159,161]

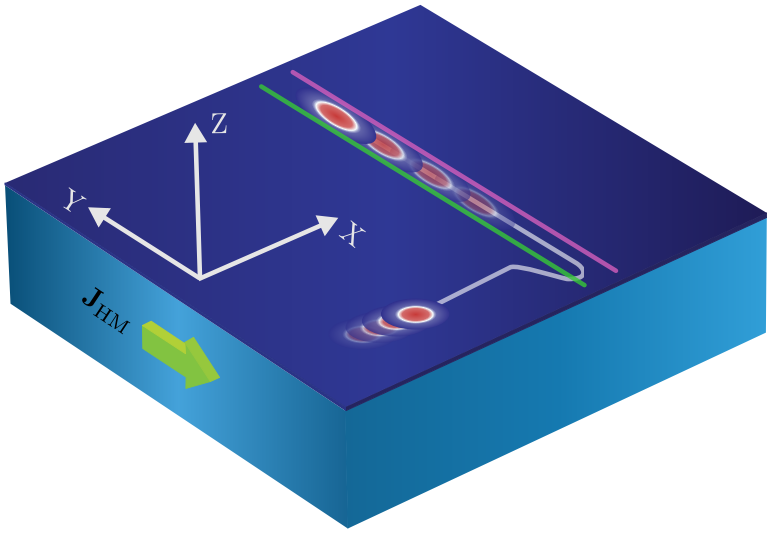

Figure 2.8: Sketch of the functioning of the skyrmionic rails. A skyrmion is driven by SHE torque and is channeled along the rails. When channeled, the skyrmion is sligthly compressed and recieves a great speed-up.

The most known approach to transport skyrmions is the skyrmion racetrack memory.[34,43] It consists of a narrow, ultrathin film where $\mathbf{J}_H$ is applied along it. Since SHE torque is proportional to $\mathbf{J}_H$ and the current is applied at the narrowest surface, the total electrical current required is much smaller. However, the SHE torque causes the skyrmion to move perpendicular to the track. Thanks to the gyrotropic nature of the skyrmion motion, the track borders not only repel the skyrmion, confining it inside the track (and nullifying the SkyHE effect), but also pushes the skyrmion along the track.[43] The skyrmion receives a speed up of the order of $1/\alpha$,[162] which usually has values around 3. One might think that this would allow skyrmions to reach a velocity of 600-900 m/s, but this is not true. The use of racetracks sets a new threshold velocity: If the skyrmion velocity is too large, it escapes the confining potential and is annihilated. This new threshold speed is also around 100-200 m/s,[71,134,162] which means that racetracks do not allow skyrmions to go faster but allow them to go as fast as without them but with lower $\mathbf{J}_H$, thus consuming less energy.

In this paper, the skyrmionic rails are presented with the same philosophy. The skyrmionic rails are a device consisting of two linear defects (local modifications of iDMI constant) engineered in a way that allow skyrmions to be accelerated, compressed, and guided along them. Skyrmionic rails outperform racetracks in terms of efficiency: they are much thinner, which would allow a higher density of skyrmion channels, and they can achieve a speed-up factor of an order of magnitude, compared with the factor 3 of racetracks.

The results show that skyrmions are guided along a channel formed by the skyrmionic rails which are thinner than the original skyrmion diameter. Moreover, the highest achieved velocity is around 180 m/s, whereas with the same applied $\mathbf{J}_H$ the skyrmion would travel at around 60 m/s along a racetrack.

Chapter 3

Rigid Model

Magnetic skyrmions are very robust magnetic structures thanks to their topological protection. The energy barriers that must be overcome to destroy them are large enough to find them in RT and have lifetimes long enough to be considered as bits of information.[163] It has been shown experimentally and theoretically by micromagnetic simulations that, although deformable, skyrmions conserve its global shape except in some extreme situations.[137,164–166] Thus, in a large number of scenearios it is a good approximation to consider the skyrmion a rigid magnetization distribution, $\mathbf{M}_0$, that translates on time over a uniform magnetization background. It can be mathematically expressed as

$$\mathbf{M}(\mathbf{r}, t) = \mathbf{M}_0(\mathbf{r} - \mathbf{r}_s(t)), \tag{3.1}$$

where $\mathbf{r}_s$ is the position of the skyrmion. This is called the rigid approximation.[54] In Fig. 3.1 it is shown that this is a good approximation for skyrmionic transport of isolated skyrmions. We can see how a skyrmion being driven by SHE torque at 50 m/s approximately conserves its shape. If we assume the rigid approximation, we can transform the LLG equation into the Thiele equation (TE),[54,71,87]

$$(\mathbb{G} - M_s\alpha\mathbb{D})\mathbf{v}_s + \gamma M_s^2\mathbf{F} = 0, \tag{3.2}$$

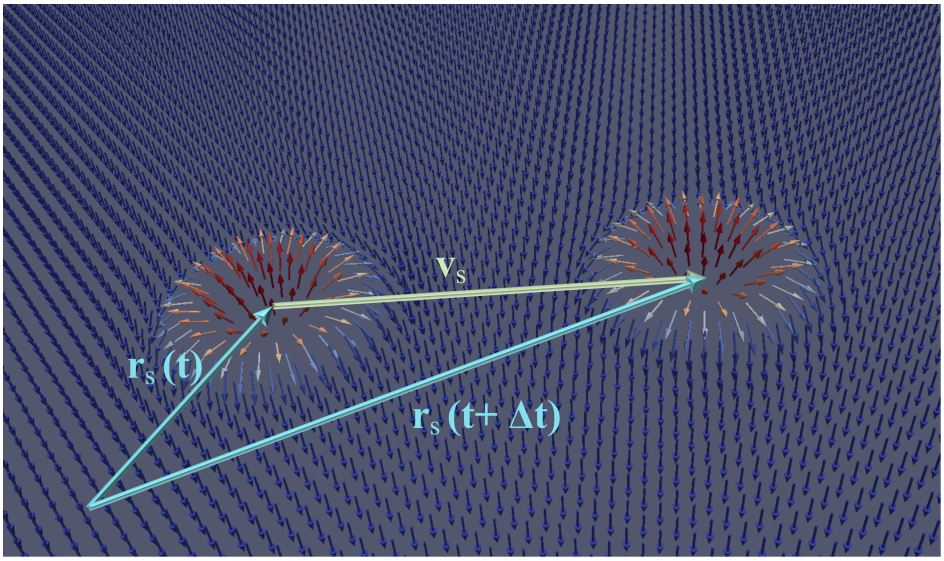

Figure 3.1: Micromagnetic simulation of the motion of an isolated skyrmion to illustrate how the skyrmion translates without deformation. Two snapshots at different times of a skyrmion being driven by SHE are shown. It can be observed that the skyrmion position changes, but its shape is not altered. The cian long vectors correpond to $\mathbf{r}_s$ at two different times, and the green vector corresponds to $\mathbf{v}_s$

where $\mathbf{v}_s = \dot{\mathbf{r}}_s$, and $\mathbb{G}$ and $\mathbb{D}$ are the gyrotropic and dissipative tensors, respectively. Both tensors depend on the magnetization distribution of the magnetic structure we are studying. The expression of its components, $\mathbb{G}_{\nu\upsilon}$, $\mathbb{D}_{\nu\upsilon}$, (ν and υ are the cartesian coordinates of the plane, x or y) are

$$\mathbb{G}_{\nu\upsilon} = \int_V \mathbf{M}_0 \cdot \left(\frac{\partial \mathbf{M}_0}{\partial \nu} \times \frac{\partial \mathbf{M}_0}{\partial \upsilon} \right) \mathrm{d}V', \tag{3.3}$$

$$\mathbb{D}_{\nu\upsilon} = \int_V \frac{\partial \mathbf{M}_0}{\partial \nu} \cdot \frac{\partial \mathbf{M}_0}{\partial \upsilon} \mathrm{d}V', \tag{3.4}$$

where V its the whole volume of the FM ultra-thin film where the skyrmion is located and $\mathrm{d}V'$ its corresponding differential of volume. In this framework, we will only consider ideal (isolated in an infinite sample), symmetric skyrmions whose core points along the +1 direction (along the z axis) while the FM background points along the -1 direction. Hence, $\mathbb{G} = \begin{pmatrix} 0 & G \\ -G & 0 \end{pmatrix}$ and $\mathbb{D} = \begin{pmatrix} D & 0 \\ 0 & D \end{pmatrix}$, being $G = 4\pi M_s^3 d$ and $D = 4\pi M_s^2 d$. $Q = G/4\pi M_s^3 d$ is known as the skyrmionic number and the fact that for ideal skyrmions $Q = \pm 1$, is the mathematical expression of the topological protection of skyrmions[158,159,167–170](structures with an integer Q are topologically protected). However, as it will be stated later, G and D also determine other characteristic phenomena of skyrmions motion.

$\mathbf{F}$ in Eq. (3.2) is the "force" term. $\mathbf{F}$ contains the effects on the skyrmion dynamics caused by the external torques in the LLG equation and all the external agents that the skyrmion may encounter, such as defects in the materials, applied magnetic field gradients, the material edges, or other magnetic structures, among others.[43,71,84,86,87,171–174] Therefore, the system that we are trying to model will determine $\mathbf{F}$.

Valuable information about the dynamics of the skyrmion can be obtained from TE even without solving it. First, TE is an ordinary differential equation (ODE) (like Newton's equation), whose solution is $\mathbf{r}_s(t)$, the trajectory of the skyrmion. However, unlike Newton's equation, it is a first-order ODE. This means that no forces are acting over the skyrmion. Those "force-terms" are actually physical magnitudes that do not have units of force and are proportional to the velocity of the skyrmion. Consequently, rigid skyrmionic dynamics[‡] do not contain inertia.[74,76,87,176,177] This means that, for example, if we are moving our skyrmion by SHE torque, when we turn off the current the skyrmion instantly stops its motion. Hence, all the interactions that skyrmions receive cause an instantaneous change in their velocity. However, as done in the literature we will continue to call $\mathbf{F}$ forces, so have in mind that from now on whenever we refer to a force acting over a skyrmion, it is actually an instantaneous change in speed.

Another important phenomenon that we can deduce from the TE is the SkyHE. Skyrmions have gyrotropic dynamics, which means that if we "push" them in one direction, they will move in a different one. This causes the well-known skyrmionic Hall angle, which is the angle between the applied $\mathbf{F}$ and $\mathbf{v}_s$.[43,71,73,92,170] This can be seen by solving the TE for an arbitrary constant force:

$$\mathbf{v}_s = -\gamma M_s^2 (\mathbb{G} - M_s \alpha \mathbb{D})^{-1} \mathbf{F}. \tag{3.5}$$

The result is that the skyrmion velocity will be the vector $\mathbf{F}$ multiplied by the matrix $-\gamma M_s^2 (\mathbb{G} - M_s \alpha \mathbb{D})^{-1}$. The matrix-vector product will cause a rotation of the vector $\mathbf{F}$ and

[‡]It has been shown[175] that small deformations can be taken into account in the TE, adding an extra term proportional to $\ddot{\mathbf{r}}_s$, thus leading to an inertial term.

since $-\gamma M_s^2(\mathbb{G} - M_s\alpha\mathbb{D})^{-1}$ is considered constant in time in the rigid model, this leads to a constant rotation of $\mathbf{F}$. The angle of this rotation is the SkyHE angle, θ_{sk}, see Fig. 3.2.

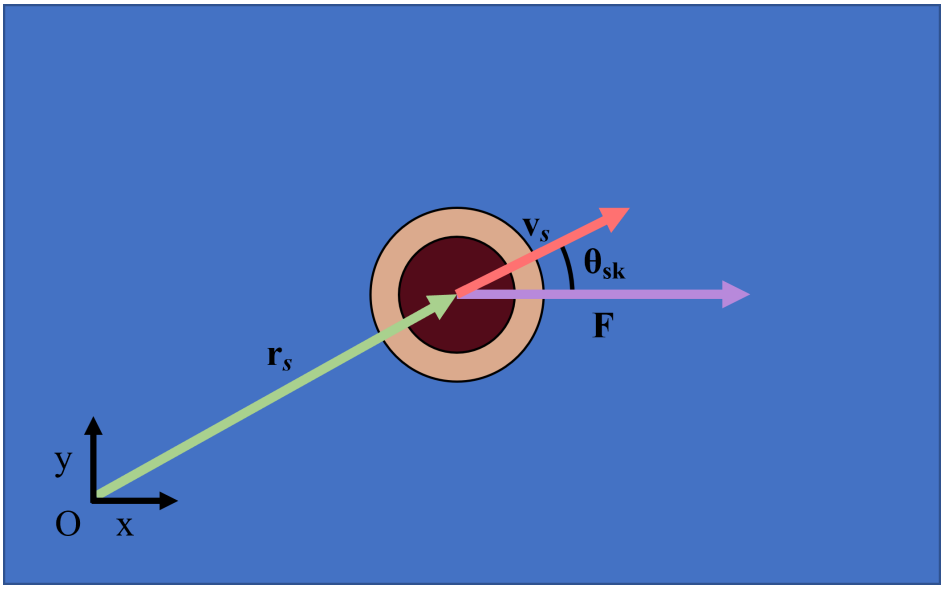

Figure 3.2: Schematic representation of the vectors $\mathbf{r}_s$, $\mathbf{v}_s$, and $\mathbf{F}$, and the skyrmionic Hall angle, θ_{sk}. The blue rectangle represents the FM background with $m_z = -1$ and the dark red circle and the brown corone represent a skyrmion at the position $\mathbf{r}_s$. This skyrmion experiments a force $\mathbf{F}$ which causes a velocity $\mathbf{v}_s$. The angle between $\mathbf{v}_s$, and $\mathbf{F}$ is the Skyrmionic Hall angle θ_{sk}.

As with micromagnetic simulations, the different terms that appear in the TE depend a lot on the system that we are modeling. To solve the TE we need to know the applied external torques, which generates an effective force on the skyrmion. For each system, we have to model the corresponding external torques and external agent forces. In particular, we will develop the STT and SHE torques that have been developed in Chapter 2, despite only using SHE in both Papers C and D. The external agents that are introduced here are the edges of the material (to model a racetrack), and atomic point defects. Both expressions will be relevant for both Papers in this chapter.

3.1 External Torques

Following the same methodology used to derive the TE one can derive the forces that the different external torques produce over the skyrmion.[43,87] We consider the skyrmion a rigid structure, Eq. (3.1), and using vectorial properties one can derive the corresponding term for each torque. The forces produced by the STT, and SHE torques, $\mathbf{F}_{\text{STT}}$ and $\mathbf{F}_{\text{SHE}}$, respectively, are:

$$\mathbf{F}_{\text{STT}} = -(\mathbb{G} - M_s\beta\mathbb{D})\mathbf{v}_F, \tag{3.6}$$

$$\mathbf{F}_{\text{SHE}} = M_s(\mathbb{N} + \zeta M_s\mathbb{Y})\mathbf{v}_H, \tag{3.7}$$

where

$$\mathbf{v}_H = -\frac{\mu_B\theta_H}{|e|M_s}(\hat{\mathbf{z}} \times \mathbf{J}_H). \tag{3.8}$$

$$\mathbb{N}_{\nu\upsilon} = \frac{1}{d}\int_V \left(\frac{\partial \mathbf{M}_0}{\partial \nu} \times \mathbf{M}_0\right)_\upsilon \mathrm{d}V', \tag{3.9}$$

$$\mathbb{Y}_{\nu\upsilon} = \frac{1}{d}\int_V \frac{\partial (\mathbf{M}_0)_\upsilon}{\partial \nu}\,\mathrm{d}V', \tag{3.10}$$

where $\mathbb{N}_{\nu\upsilon}$ and $\mathbb{Y}_{\nu\upsilon}$ are the components of the tensors $\mathbb{N}$ and $\mathbb{Y}$.

3.2 External Forces

Modelling the forces that external agents do over skyrmions, $\mathbf{F}_{\text{ext}}$, is not as straight forward as modeling the forces of the external torques. The components of this force, $(\mathbf{F}_{\text{ext}})_i$, can be calculated by,[54,71]

$$(\mathbf{F}_{\text{ext}})_\nu = \int_V \mathbf{H}_{\text{ext}} \cdot \frac{\partial \mathbf{M}_0}{\partial \nu}\,\mathrm{d}V, \tag{3.11}$$

where $\mathbf{H}_{\text{ext}}$ is the field generated by the external agent. The difficulty here lies in calculating such field: what is the effective field generated by a material edge or an atomic defect, for example?

Edge of the material & racetrack

Within the MM the edges of the racetrack are modeled with boundary conditions. This means that the effective field can not be computed at the edges of the material. Hence we can not use Eq. (3.11) to compute the corresponding force. To solve this problem, different approaches have been used. In particular we will use the expression found in Ref. [71], where a mathematical expression is found empirically and adjusted via energy minimization.

Upon reaching the material edge, the skyrmion is repelled by it. Due to the gyrotropic nature of the skyrmionic dynamics, the skyrmion also experiences a force parallel to the track which usually speeds it up. All this has been observed both experimentally and theoretically through MM simulations.[34,37,43,74,86,114,162,178–182]Thus, it can be empirically deduced that the force that the edge of the material exerts over a skyrmion, $\mathbf{F}_{\text{Ed}}$, should have the following shape:

$$\mathbf{F}_{\text{Ed}} = F_{\text{Ed}}(d_{\text{sk}-\text{Ed}})\hat{\mathbf{n}}, \tag{3.12}$$

where $F_{\text{Ed}}(d_{\text{sk}-\text{Ed}})$, the modulus of the force, is a decreasing function of $d_{\text{sk}-\text{Ed}}$, the distance between the edge of the material and the skyrmion, and $\hat{\mathbf{n}}$ is the unitary vector normal to the edge. Using an energy-minimizing method the force expression is found,

$$\mathbf{F}_{\text{Ed}} = f_0 e^{-(d_{\text{sk}-\text{Ed}})}\hat{\mathbf{n}}, \tag{3.13}$$

where f_0 is a constant that depends on the material parameters, the skyrmion shape, and size. This expression is crucial in the modelling of skyrmionic systems since the most famous skyrmionic device is the skyrmionic racetrack memory,[34] which basically consists in a narrow strip of FM material which channels the skyrmions thanks to the confining potential of its edges. Hence, the force that a racetrack parallel to the x axis of width $2W$ generates on a skyrmion, $\mathbf{F}_R$ is,

$$\mathbf{F}_R = \mathbf{F}_{\text{Ed}}(y+W) + \mathbf{F}_{\text{Ed}}(y-W) = f_0\left[e^{-(y+W)} - e^{-(y-W)}\right]\hat{\mathbf{y}}. \tag{3.14}$$

This is the expression used to model racetracks in both, Papers C and D. The effect that it

has over a skyrmion is sketched in Fig. 3.3 with and without applied curred. In Fig. 3.3-a/b we can see the force field that a track generates without/with applied current. In Fig. 3.3-c/d we see the equilvanet $\mathbf{v}_s$ caused by this force without/with applied current. We can see how the skyrmion is repelled by the edges of the material and how, thanks to the gyrotropic nature of the skymion dynamics, this translates in the skyrmions being channeled along the racetrack. Notice that Fig. 3.3 is a sketch of the scenario where $\mathbf{v}_H$ is not large enough to overcome the confining potential.

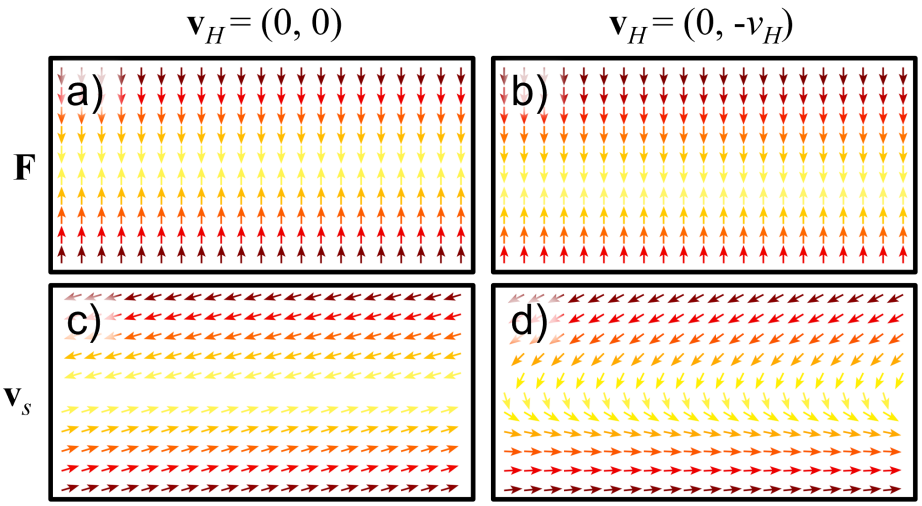

Figure 3.3: Schematic representation of vectorials fields $\mathbf{F}$ and $\mathbf{v}_s$. The darker the arrow, the more intense the magnitude is, where the vectors are hard to see, the magnitude is almost 0. a) $\mathbf{F}$ if we had a racetrack formed by two edges of the material separated by a distance $2W$. b) Same than a) adding $\mathbf{v}_H = (0, -v_H)$, where v_H is a positive constant. c)/d) $\mathbf{v}_s$ generated by the $\mathbf{F}$ displayed in a)/b).

Atomic Point Defect

An atomic point defect is an absence or the substitution of one atom of the ferromagnet by a different one, causing a local variation of the physical parameters of the system. In Ref. [86], the effective field due to an atomic point defect in a system such as the one treated in this thesis (ultrathin FM film, considering exchange, anisotropy, and iDM interaction), and considering a square lattice with lattice parameter a, was found to be

$$\mathbf{H}_{\text{at}} = \frac{|\boldsymbol{\mu}|^2 \delta(\mathbf{r} - \mathbf{r}_d)}{\mu_0 M_s^2 d} \left[\frac{(\delta_{\text{ex}} - 1) J a^2}{2} \nabla^2 \mathbf{M} + (\delta_{\text{an}} - 1) K M_z \hat{\mathbf{z}} + \right. \\ \left. + (\delta_{\text{DM}} - 1) |\mathbf{D}_{ij}| a \left[(\nabla \mathbf{M}) \hat{z} - \nabla M_z \right] \right] \tag{3.15}$$

where δ_{ex}, δ_{an}, and δ_{DM} are the fraction of variation of the exchange, anisotropy, and iDMI parameters, respectively. $\delta(\mathbf{r})$ is the Dirac delta and $\mathbf{r}_d$ is the position of the defect. The force that a point atomic defect causes on an ideal skyrmion of radius R is [after Eq. (3.11)]:

$$\mathbf{F}_{\text{at}} = \frac{4|\boldsymbol{\mu}|^2 R^2 \gamma}{\mu_0 M_s d} \left[\frac{2|\mathbf{D}_{ij}|(\delta_{\text{DM}} - 1) a R r_s}{(R^2 + r_s^2)^3} - \frac{K(\delta_{\text{an}} - 1) r_s (R^2 - r_s^2)}{(R^2 + r_s^2)^3} \right] \hat{\mathbf{r}}, \tag{3.16}$$

where R is the radius of the skyrmion and $r_s = |\mathbf{r}_s|$. This expression is used to justify the

expression used for a punctual pinning in Paper C and it is the starting point to model granularity in Paper D. The effect of an atomic defect of iDMI, located at the center of each figure, would have on a skyrmion is sketched in Fig. 3.4 with and without applied current. In Fig. 3.4-a/b we can see the force field that a atomic point defect generates without/with applied current. In Fig. 3.4-c/d we see the equivalent $\mathbf{v}_s$ caused by this force without/with applied current. We can see how the skyrmion is attracted by the defect and how thanks to the gyrotropic nature of the skymion dynamics this translates in the skyrmions following a spiral-like trajectory around it. Notice that Fig. 3.4 is a sketch of the scenario where $\mathbf{v}_H$ is not large enough to overcome the pinning potential.

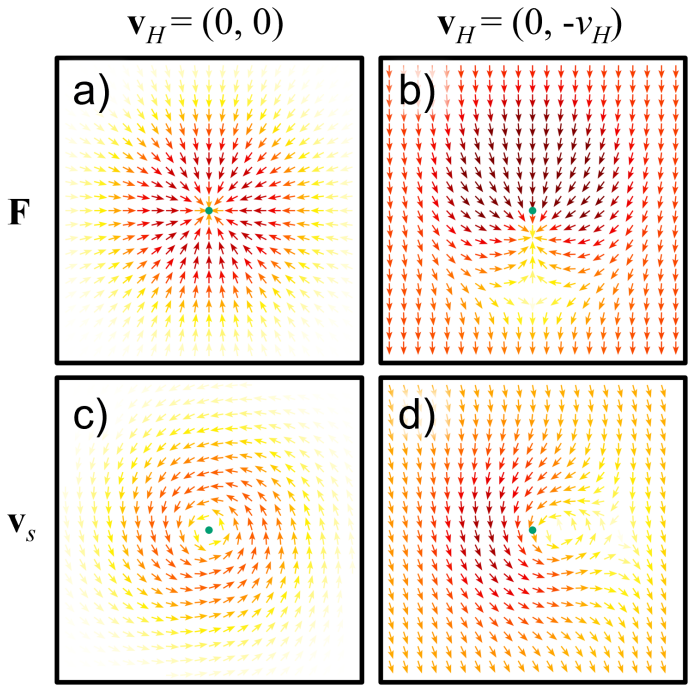

Figure 3.4: Schematic representation of vectorials fields $\mathbf{F}$ and $\mathbf{v}_s$. The darker the arrow, the more intense the magnitude is, where the vectors are hard to see, the magnitude is almost 0. a) $\mathbf{F}_{\text{at}}$ with $\kappa = 0, \delta < 0$. b) Same than a) adding $\mathbf{v}_H = (0, -v_H)$, where v_H is a positive constant. c)/d) v_s generated by the $\mathbf{F}$ displayed in a)/b).

3.3 Thermal Effects and the Stochastic Thiele Equation

Most of the work done up to now by theoreticians in the skyrmionic field has been done without considering the thermal effects. This is due to the enormous complexity that temperature adds to the system. Moreover, ferromagnetism is a temperature-dependent phase state, so even the macroscopic properties of the material could change depending on the order of magnitude of the temperature.[52,53] In spite of this, the effect that the temperature has on the skyrmion dynamics within the rigid model can be modeled by a force, $\mathbf{F}_T$.[53] Let's go back to the beginning. If we consider a FM ultrathin film, it remains FM if its temperature is below its Curie temperature, T_C. One of the assumptions of the MM is that $|\mathbf{M}| = M_s$ is a constant, however, it is well-known that M_s depends strongly on the temperature.[52,53] Hence, to model a FM film at $0 \neq T \ll T_C$, it can be considered that M_s variations are not relevant. If these conditions are met, we can consider that the temperature causes a stochastic effective field, $\mathbf{H}_T$, which can be added to the MM. This is known as the stochastic MM. To obtain

relevant results from stochastic simulations one might perform a large number of simulations and average over them to obtain statistically relevant results.

$\mathbf{H}_T$ is an stochastic field described by a Gaussian noise with the following properties:

$$\langle H_{T,\nu}(t)\rangle = 0, \tag{3.17}$$

$$\langle H_{T,\nu}(t)H_{T,\upsilon}(t')\rangle = \frac{\xi}{V}\delta_{\nu\upsilon}\delta(t-t'), \tag{3.18}$$

where $\langle\rangle$ are the averages over time, the subscripts ν, υ refer to the Cartesian components, $\delta_{\nu\upsilon}$ is the Kronecker delta, $\delta(t-t')$ is the Dirac delta, and $\xi{=}\frac{2\alpha k_B T}{\gamma\mu_0 M_s}$, being k_B the Boltzmann constant.[53,130,156] From this stochastic field, one can compute the associated stochastic force, $\mathbf{F}_{\text{st}}$ that this field makes on a skyrmion using Eq. (3.11),

$$(\mathbf{F}_{\text{st}})_\nu = \int_V \mathbf{H}_T \frac{\partial \mathbf{M}_0}{\partial \nu} \mathrm{d}V'. \tag{3.19}$$

Hence, $\mathbf{F}_{\text{st}}$ will also be described by a Gaussian noise, whose properties will be,

$$\langle F_{\text{st},\nu}\rangle = \int_V \langle \mathbf{H}_T\rangle \frac{\partial \mathbf{M}_0}{\partial \nu}\mathrm{d}V' = 0, \tag{3.20}$$

$$\begin{aligned}\langle F_{\text{st},\nu}(t)F_{\text{st},\upsilon}(t')\rangle &= \int_V\int_V \langle H_{T,\nu}(t)H_{T,\upsilon}(t')\rangle \frac{\partial \mathbf{M}_0}{\partial \nu}\frac{\partial \mathbf{M}_0}{\partial \upsilon}\mathrm{d}V'\mathrm{d}V'' \simeq \\ &\simeq \xi D\delta_{\nu\upsilon}\delta(t-t').\end{aligned}$$

In summary, the Thiele equation of a skyrmion driven by damping-like torques, produced by spin-polarized currents arising from the SHE after feeding an in-plane current into a heavy-metal substrate, in the presence of arbitrary external agents and at an arbitrary temperature is,[130]

$$(\mathbb{G} - M_s\alpha\mathbb{D})\mathbf{v}_s + M_s\mathbb{N}\mathbf{v}_H + \gamma M_s^2(\mathbf{F}_{\text{ext}} + \mathbf{F}_{\text{st}}) = 0. \tag{3.21}$$

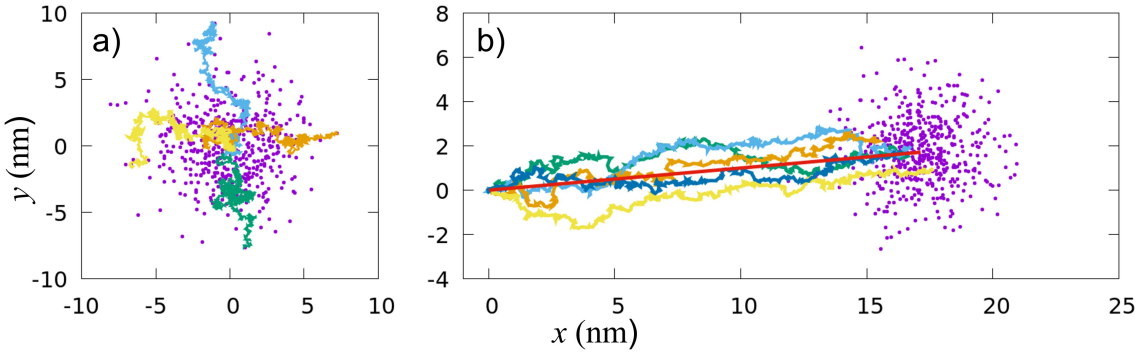

Figure 3.5: Solutions of the STE at RT with the parameters of Paper C, with no external agents present with a) $\mathbf{v}_H = (0,0)$, b) $\mathbf{v}_H = (600,0)$ m/s. The colored lines represent 5 particular solutions of the STE. The red line corresponds to the solution of $T = 0$. The purple dots are the final position of 500 simulations with the same simulation time. The simulation times are a) 0.8 ns b) 0.4 ns. Note that different solutions are found for the same equation due to its stochastic nature.

This equation also called the stochastic Thiele equation (STE). It is an stochastic ODE that describes the motion of a body subjected to a combination of deterministic and stochastic forces. Some solutions of this equation are shown in Fig. 3.5. Notice that, as with the stochastic MM model, to obtain statistically significant results, a large number of simulations must be performed and the results obtained averaged. This leads to a prohibitive computational time if results with high accuracy are to be obtained.

Eq. (3.21) is the starting point of Paper C. From this equation, a deterministic approach is developed which consists in solving a single PDE, hence it only requires one single simulation. The same deterministic approach is used in Paper D.

3.4 Papers

In this thesis, two papers focus on the rigid model. In Paper C we have presented a deterministic approach for studying the skyrmion dynamics with $T \neq 0$ that consists in solving the Fokker-Plank equation (FPE) of the skyrmion. This approach outperforms the STE, Fig. 3.6. The solution of the FPE is the probability of finding a skyrmion at a given position and time, Fig. 3.7. Paper D uses this deterministic approach to determine the feasibility of the original track when considering thermal effects and granularity simultaneously, scheme in Fig. 3.8 and results in Fig. 3.9. The methodology followed in Paper D has the best, to the best of our knowledge, realistic/numerical performance ratio for simulating skyrmionic devices reached up to now.

3.4.1 Paper C

The incorporation of temperature effects in modeling nano- and micromagnetic systems is a difficult challenge for theorists. The main theoretical models, ranging from the lowest to the broadest length scale are the stochastic atomistic model (SSAM), the stochastic MM, the Landau-Lifshitz-Bloch (LLB) model, and the STE model.

In the SSAM,[53] there is no extra assumption in comparison with the regular atomistic model. It is only assumed that the system is under a thermal bath of temperature T. As a consequence, an extra effective field is generated, which makes the atomic moments "jiggle". It is the most accurate model from the physical point of view and all the models to be presented later are derived from it. The major drawback is the extremely high computational power required. For example, to simulate a skyrmion at RT (they usually have a $R \sim 100$nm) requires about 10^6 magnetic moments, in contrast to the 10^4 required in the stochastic MM or the LLB model. This, of course, scales exponentially as the system grows to make the simulation of the skyrmion dynamics at RT not feasible.

The stochastic MM is perhaps the most widely used of all. It is derived from the SSAM, but as already mentioned, it is only valid in a certain temperature range (around $T < \frac{1}{3}T_C$), where considering M_s approximately constant is a valid approximation. In spite of this, the nucleation, annihilation, and dynamics of skyrmions can be studied (the T_C of Co is 1400K approximately), but some phenomena, such as the ferromagnetic-paramagnetic transition of a system, cannot be studied with the same accuracy. The computational power required to perform a single stochastic MM simulation is higher than that of a regular MM, but of the same order of magnitude.

The LLB model is also derived from the SSAM and solves most of the drawbacks of the stochastic MM. Using a mean field approximation, the effective fields are modified, and some

extra terms are added to the LLG equation. As a result, one obtains a model that is almost as valid as the SSAM (only the mean-field approximations are made), and much more accurate than the stochastic MM. There is a family of these methods, but the one currently in use is also a stochastic method. Although it is a much more accurate version of the stochastic MM, it is barely used due to its complexity. In addition to a more complex set of PDEs, a large set of parameters is needed to use the model, which requires several previous SSAM or density-functional theory calculations. The computational power required for this method is higher than the stochastic MM but on the same order of magnitude.

The STE is derived from the stochastic MM, with the extra assumptions of the rigid model. Therefore, not only does the system need to be far from T_C, but also the energy barrier of the skyrmionic state must be much larger than k_BT. For some systems it has been shown that skyrmions' lifetime at RT is long enough to be considered for spintronic applications, so it would be safe to use STE. STE requires much less computational power than stochastic MM but has the same drawbacks as the regular TE compared to the regular MM. The generation, deformation, and annihilation processes of the skyrmion can not be simulated or taken into account in the dynamics. The STE and all the methods aforementioned are stochastic. This means that a large number of simulations have to be performed and then averaged to obtain meaningful results.

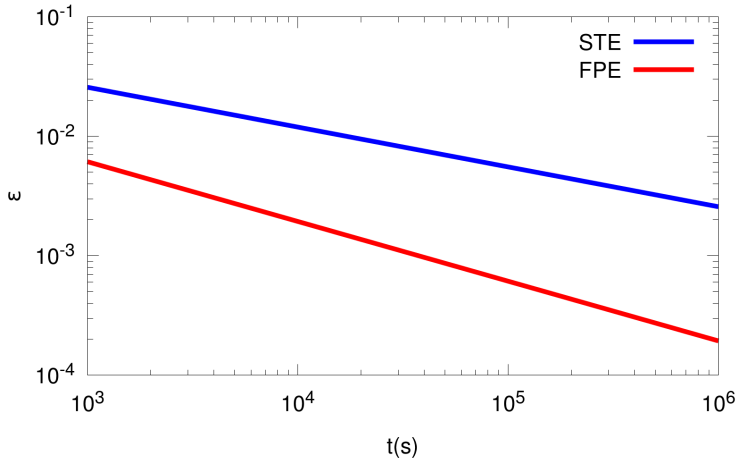

Figure 3.6: Comparisson of the total error of both methods (statistical + numerical) as a function of the simulation time when the mesh size is fixed. We can see that the error is about an order of magnitude lower for the FPE, and as the simulation time increases, the error decreses even faster. Notice that the scale is logarithmic.

Fortunately, the STE is a Langevin equation, and the corresponding FPE can be derived. The FPE of a body is a PDE whose solution is the probability density of finding that object at a given position and time, thus it is a deterministic equation. The only condition is that the object in motion, in this case, the skyrmion, follows a Brownian-like motion. This is the case for skyrmions, and it has been shown both experimentally and theoretically.[130,137]

In Paper C the FPE of a skyrmion [the corresponding FPE of the STE introduced in Eq. (3.21)] is derived. The advantages of this model compared with the other ones presented here are shown, Fig. 3.6. For this purpose, the motion of a skyrmion moving near a pining center, Fig. 3.7, and the motion of a skyrmion along a racetrack are simulated as examples. Compared to the STE, the FPE is a much more efficient method since its solution is equivalent

to the average of infinitely many STE solutions. Furthermore, the STE is a transport equation that can be easily solved with relatively simple numerical methods and commercial software.

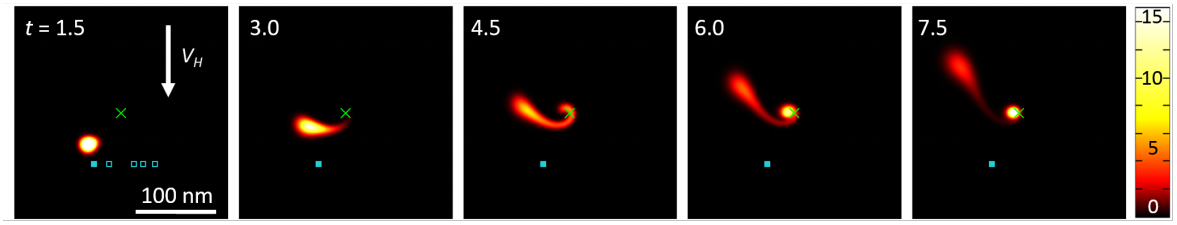

Figure 3.7: Solution of the FPE of a skyrmion approaching a pinning potential (green cross) for different times. The brigther it is the spot, the more likely it is to find a skyrmion there. We can see how the binarity of the dynamics are broken: there is a probability that the skyrmion is trapped by the pinning or that the skyrmions escapes the potential.

3.4.2 Paper D

Skyrmions have been a hot topic for the last decade due to their promising properties. Skyrmionic devices have been proposed for stochastic computing, neuromorphic computing, information transport, processing, and storage... As the list grows and scientists bring these devices closer to reality, realistic simulations become essential.

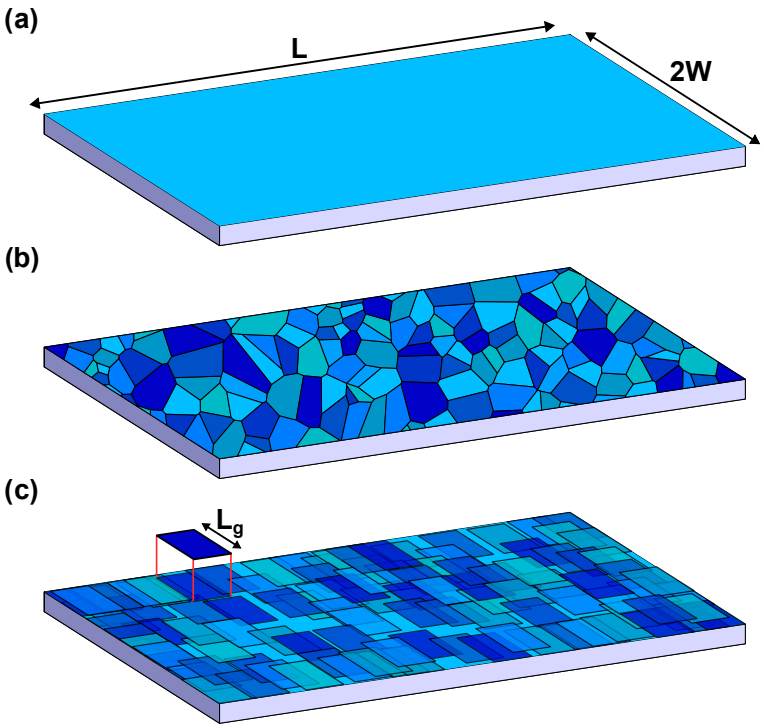

Figure 3.8: Scheme of the modeled system in Paper D. There are 3 samples: a) the plain sample, without granularity, b) a granular sample, represented by a Voronoi tesselation, c) how the granularity is geometrically simplified to obtain simpler, yet equivalent, mathematical expressions.

MM has proved to be adequate and useful for the simulation of simple application designs, as in paper B, mainly because they have a great trade-off between realism and computational cost. However, the designs are becoming much more complex and the accuracy margin is becoming much thinner. Moreover, as we include more ingredients in the MM, the computational power required for the simulations escalates exponentially. Real skyrmionic systems are granular, Fig. 3.8, and most importantly, if they are ever to be real devices, they have to run at RT. Including these two phenomena in the MM is too costly.

In Paper D, one of the most realistic simulations of a skyrmionic device is done, with a realistic computational time. To do so, we model the granularity of a system within the rigid model, computing the effective force generated over the skyrmion. Then we solve the FPE of skyrmion moving along a granular racetrack at RT, Fig. 3.9. From the results, we calculate some key magnitudes like the probabilities of success of the transport of information.

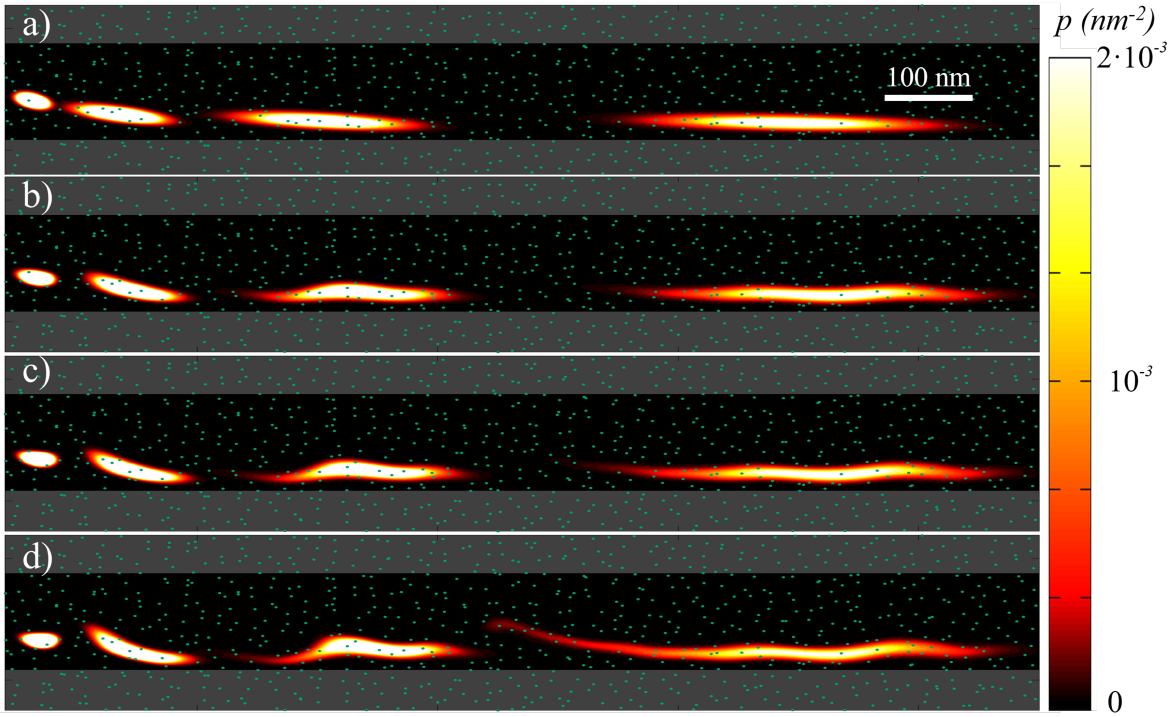

Figure 3.9: Solution of the FPE of a skyrmion being transported along a granular racetrack at RT. Different snapshots of the probability density function are shown for each track. The amount of grains is the same in the 4 plots and the variation of physical parameters between grains increases from a) to d).

The results from this work establish the viability of the skyrmionic racetrack memories, highlighting a few flaws in the device, and indicating how they could be fixed. Moreover, we also present a methodology that can be used for realistic and efficient simulations of heavily complex skyrmionic systems, like some of the new skyrmionic devices designed.[38,183–186]

Chapter 4

Conclusions & Final remarks

This thesis focuses on the theoretical study of skyrmionic devices, a type of spintronic device that employs skyrmions as the building blocks. Skyrmions are a magnetic structure with remarkable properties, such as being small, easy to move, and highly stable. As a result, skyrmionic devices have the potential to significantly contribute to the development of more powerful and environmentally friendly data centers and computers.

The field of skyrmions is relatively recent, since it skyrocketed after the theoretical proposal of the racetrack memory[34] in 2013. Several advances have been made, but there are still many obstacles to overcome before skyrmionic devices can become a reality, let alone be commercialized. In this thesis we contributed to this field with a set of new theoretical tools (Paper A and C), designing a new device (Paper B) and optimizing and checking the feasibility in realistic conditions of the racetrack memory (Paper D).

Although the papers in this thesis have been grouped into two chapters based on the theoretical model used, there is a stronger argument for separating Paper A from Papers B, C, and D based on subject matter. Paper A addresses a highly specific problem that was encountered during the development of the other papers and is more numerically and technically oriented. In contrast, Papers B, C, and D center around the primary topic of this thesis: optimizing the transport of skyrmions.

Paper B presents the skyrmionic rails, a device that achieved the highest efficiency in terms of skyrmionic transport at the time of its publication. However, the experimental implementation of such a device would require cutting-edge technology, as it necessitates the modification of the HM substrate of the system with a precision on the order of nanometers.

Micromagnetic simulations have been one of the main tools of theoreticians in the field of solid magnetism. However, experimentalists sometimes find them inaccurate and unrealistc. This is because many things are ignored when using the MM, for the sake of simplicity and computational efficiency, which are sometimes relevant. The main two factors that are ignored are the thermal effects and the inhomogeneities of the material or granularity. We aimed to bridge this gap providing a computationally efficient method to include both, the granularity and the thermal effects.

In paper C, we present the skyrmion's FPE, the most computationally efficient model that includes the thermal effects in the skyrmionic dynamics. In contrast with the other presented methods, it is a deterministic model, hence, does not require to solve an equation multiple times and a posterior statistical analysis. The only drawback is that we have to consider the skyrmion as a rigid structure. But, as a matter of fact, if we can not achieve rigid enough skyrmions at RT, skyrmionic devices will not be a reality.

In paper D we add the granularity to the model presented in paper C. We study the viability of the racetrack memory finding some carences of the system (that can be fixed). The simulations done in this work have the highest reality/complexity ratio in the literature. Moreover, the methodology consists in solving a deeply studied and very standard PDE that can be solved with many popular softwares. We believe that if the scientific community would give a try to our model, they would find a much more efficient substitute to the STE.

Continuing with the work done in Paper C and D, there is still more to be done to make the model more realistic. For example, it has been reported that the diffusion coefficient introduced in Paper C does not depend lineraly with the temperature.[130] Also, a correction to D has been done when working at $T \neq 0$.[187] Both these corrections (and any other correction that is done to the STE) could be included in our model, without adding any extra layer of complexity.

Step by step, the skyrmionic community will keep working to make the skyrmionic devices feasible. Some members of the scientific community say that skyrmions might be a transitory hot topic that will decay with time. They might be right. Skyrmionic systems are based in rare metals and materials like the platinum and iridium. Individual skyrmion motion is still really hard to controll experimentally. Experiments show general trends, but not the extreme accuracy that we expect from a data storage system. However, even in the worst scenario, where skyrmionic devices are proven to be unviable, many significant advances in many fields would have been done: in the theoretical studies of magnetic textures at the sub micrometer length scale, the experimental manipulation of such structures through external torques and magnetic fields, new material systems like the HM-FM multilayers or other interfacial systems...

There is also room for optimism as the field has advanced at breakneck speed. Major hurdles have already been overcome so there is no reason not to be confident that the scientific community can continue to do so. And, if we are capable to do it, the reward would be extraordinary: the implementation of skyrmionic devices would have the potential of revolutionise the landscape of IT.

And what is certain is that, sooner or later, a way will be found to sustain our technological growth without compromising our planet, and fortunately, I will have contributed my grain of sand.

List of Figures

Bibliography

[1] C. E. Shannon. A mathematical theory of communication. *The Bell System Technical Journal*, 27:623–656, 1948.

[2] D. Silver, J. Schrittwieser, K. Simonyan, I. Antonoglou, A. Huang, A. Guez, T. Hubert, L. Baker, M. Lai, A. Bolton, Y. Chen, T. Lillicrap, F. Hui, L. Sifre, G. V. D. Driessche, T. Graepel, and D. Hassabis. Mastering the game of go without human knowledge. *Nature*, pages 354–359, 10 2017.

[3] F. Giust, L. Cominardi, and C. Bernardos. Distributed mobility management for future 5g networks: Overview and analysis of existing approaches. *IEEE Communications Magazine*, 53:142–149, 1 2015.

[4] P. Hamet and J. Tremblay. Artificial intelligence in medicine. *Metabolism*, 69:S36–S40, 4 2017.

[5] · Moore's law-now and in the future. 10.1109/N-SSC.2006.4785860. `https://www.intel.com/content/www/us/en/newsroom/opinion/moore-law-now-and-in-the-future.html`.

[6] G. E. Moore. Cramming more components onto integrated circuits, reprinted from electronics, volume 38, number 8, april 19, 1965, pp.114 ff. *IEEE Solid-State Circuits Society Newsletter*, 11(3):33–35, 2006.

[7] C. A. MacK. Fifty years of moore's law. *IEEE Transactions on Semiconductor Manufacturing*, 24:202–207, 5 2011.

[8] N. Jones. How to stop data centres from gobbling up the world's electricity. *Nature*, 561:163–166, 9 2018.

[9] S. Bhatti, R. Sbiaa, A. Hirohata, H. Ohno, S. Fukami, and S. N. Piramanayagam. Spintronics based random access memory: a review. *Materials Today*, 20:530–548, 11 2017. 10.1016/J.MATTOD.2017.07.007.

[10] I. Žutić, J. Fabian, and S. D. Sarma. Spintronics: Fundamentals and applications. *Reviews of Modern Physics*, 76:323, 4 2004. 10.1103/RevModPhys.76.323.

[11] V. E. Demidov, S. Urazhdin, G. de Loubens, O. Klein, V. Cros, A. Anane, and S. O. Demokritov. Magnetization oscillations and waves driven by pure spin currents. *Physics Reports*, 673:1–31, 2 2017. 10.1016/J.PHYSREP.2017.01.001.

[12] M. Johnson and R. H. Silsbee. Interfacial charge-spin coupling: Injection and detection of spin magnetization in metals. *Physical Review Letters*, 55:1790, 10 1985. 10.1103/PhysRevLett.55.1790.

[13] S. Datta and B. Das. Electronic analog of the electro-optic modulator. *Applied Physics Letters*, 56:665, 6 1998. 10.1063/1.102730.

[14] M. N. Baibich, J. M. Broto, A. Fert, F. N. V. Dau, F. Petroff, P. Eitenne, G. Creuzet, A. Friederich, and J. Chazelas. Giant magnetoresistance of (001)fe/(001)cr magnetic superlattices. *Physical Review Letters*, 61:2472–2475, 11 1988. 10.1103/PHYSREVLETT.61.2472/FIGURE/1/THUMB.

[15] G. Binasch, P. Grünberg, F. Saurenbach, and W. Zinn. Enhanced magnetoresistance in layered magnetic structures with antiferromagnetic interlayer exchange. *Physical Review B*, 39:4828, 3 1989. 10.1103/PhysRevB.39.4828.

[16] D. D. Awschalom and M. E. Flatté. Challenges for semiconductor spintronics. *Nature Physics*, 3:153–159, 3 2007. 10.1038/nphys551.

[17] M. Hayashi, L. Thomas, R. Moriya, C. Rettner, and S. S. Parkin. Current-controlled magnetic domain-wall nanowire shift register. *Science*, 320:209–211, 4 2008. 10.1126/science.1154587.

[18] S. S. Parkin, M. Hayashi, and L. Thomas. Magnetic domain-wall racetrack memory. *Science*, 320:190–194, 4 2008. 10.1126/science.1145799.

[19] R. Hanson, L. P. Kouwenhoven, J. R. Petta, S. Tarucha, and L. M. Vandersypen. Spins in few-electron quantum dots. *Reviews of Modern Physics*, 79:1217–1265, 10 2007. 10.1103/REVMODPHYS.79.1217/FIGURES/49/MEDIUM.

[20] D. Marković, A. Mizrahi, D. Querlioz, and J. Grollier. Physics for neuromorphic computing. *Nature Reviews Physics*, 2:499–510, 7 2020. 10.1038/s42254-020-0208-2.

[21] J. Grollier, D. Querlioz, K. Y. Camsari, K. Everschor-Sitte, S. Fukami, and M. D. Stiles. Neuromorphic spintronics. *Nature Electronics*, 3:360–370, 3 2020. 10.1038/s41928-019-0360-9.

[22] S. Peng, D. Zhu, J. Zhou, B. Zhang, A. Cao, M. Wang, W. Cai, K. Cao, and W. Zhao. Modulation of heavy metal/ferromagnetic metal interface for high-performance spintronic devices. *Advanced Electronic Materials*, 5:1900134, 8 2019. 10.1002/AELM.201900134.

[23] Y. Tokura and N. Kanazawa. Magnetic skyrmion materials. *Chemical Reviews*, 121:2857–2897, 3 2021. 10.1021/acs.chemrev.0c00297.

[24] S. Mühlbauer, B. Binz, F. Jonietz, C. Pfleiderer, A. Rosch, A. Neubauer, R. Georgii, and P. Böni. Skyrmion lattice in a chiral magnet. *Science (New York, N.Y.)*, 323(5916):915–9, feb 2009. 10.1126/science.1166767.

[25] X. Z. Yu, Y. Onose, N. Kanazawa, J. H. Park, J. H. Han, Y. Matsui, N. Nagaosa, and Y. Tokura. Real-space observation of a two-dimensional skyrmion crystal. *Nature*, 465(7300):901–4, jul 2010. 10.1038/nature09124.

[26] T. H. Skyrme. A unified field theory of mesons and baryons. *Nuclear Physics*, 31:556–569, 3 1962. 10.1016/0029-5582(62)90775-7.

[27] T. L. Ho. Spinor bose condensates in optical traps. *Physical Review Letters*, 81:742, 7 1998. 10.1103/PhysRevLett.81.742.

[28] D. C. Wright and N. D. Mermin. Crystalline liquids: the blue phases. *Reviews of Modern Physics*, 61:385, 4 1989. 10.1103/RevModPhys.61.385.

[29] M. Abolfath, J. J. Palacios, H. A. Fertig, S. M. Girvin, and A. H. MacDonald. Critical comparison of classical field theory and microscopic wave functions for skyrmions in quantum hall ferromagnets. *Physical Review B*, 56:6795, 9 1997. 10.1103/PhysRevB.56.6795.

[30] S. L. Sondhi, A. Karlhede, S. A. Kivelson, and E. H. Rezayi. Skyrmions and the crossover from the integer to fractional quantum hall effect at small zeeman energies. *Physical Review B*, 47:16419, 6 1993. 10.1103/PhysRevB.47.16419.

[31] A. Fert, N. Reyren, and V. Cros. Magnetic skyrmions: advances in physics and potential applications. *Nature Reviews Materials*, 2(7):17031, jun 2017. 10.1038/natrevmats.2017.31.

[32] K. Everschor-Sitte, J. Masell, R. M. Reeve, and M. Kläui. Perspective: Magnetic skyrmions—Overview of recent progress in an active research field. *Journal of Applied Physics*, 124(24):240901, dec 2018. 10.1063/1.5048972.

[33] A. N. Bogdanov and D. Yablonskii. Thermodynamically stable "vortices" in magnetically ordered crystals. the mixed state of magnets. *Journal of Experimental and Theoretical Physics*, 95(1):178, 1989.

[34] A. Fert, V. Cros, and J. Sampaio. Skyrmions on the track. *Nature Nanotechnology*, 8(3):152–6, mar 2013. 10.1038/nnano.2013.29.

[35] G. Bourianoff, D. Pinna, M. Sitte, and K. Everschor-Sitte. Potential implementation of reservoir computing models based on magnetic skyrmions. *AIP Advances*, 8(5):055602, may 2018. 10.1063/1.5006918.

[36] R. Wiesendanger. Nanoscale magnetic skyrmions in metallic films and multilayers: a new twist for spintronics. *Nature Reviews Materials*, 1(7):16044, jul 2016. 10.1038/natrevmats.2016.44.

[37] X. Zhang, M. Ezawa, and Y. Zhou. Magnetic skyrmion logic gates: conversion, duplication and merging of skyrmions. *Scientific Reports*, 5:9400, jan 2015. 10.1038/srep09400.

[38] J. Zázvorka, F. Jakobs, D. Heinze, N. Keil, S. Kromin, S. Jaiswal, K. Litzius, G. Jakob, P. Virnau, D. Pinna, K. Everschor-Sitte, L. Rózsa, A. Donges, U. Nowak, and M. Kläui. Thermal skyrmion diffusion used in a reshuffler device. *Nature Nanotechnology*, 14(7):658–661, apr 2019. 10.1038/s41565-019-0436-8.

[39] N. Romming, A. Kubetzka, C. Hanneken, K. von Bergmann, and R. Wiesendanger. Field-dependent size and shape of single magnetic Skyrmions. *Physical Review Letters*, 114(17):177203, may 2015. 10.1103/PhysRevLett.114.177203.

[40] R. Tomasello, K. Y. Guslienko, M. Ricci, A. Giordano, J. Barker, M. Carpentieri, O. Chubykalo-Fesenko, and G. Finocchio. Origin of temperature and field dependence of magnetic skyrmion size in ultrathin nanodots. *Physical Review B*, 2018. 10.1103/PhysRevB.97.060402.

[41] D. Cortés-Ortuño, W. Wang, M. Beg, R. A. Pepper, M.-A. Bisotti, R. Carey, M. Vousden, T. Kluyver, O. Hovorka, and H. Fangohr. Thermal stability and topological protection of skyrmions in nanotracks. *Scientific Reports*, 7(1):4060, dec 2017. 10.1038/s41598-017-03391-8.

[42] S. Woo, K. Litzius, B. Krüger, M.-Y. Im, L. Caretta, K. Richter, M. Mann, A. Krone, R. M. Reeve, M. Weigand, P. Agrawal, I. Lemesh, M.-A. Mawass, P. Fischer, M. Kläui, and G. S. D. Beach. Observation of room-temperature magnetic skyrmions and their current-driven dynamics in ultrathin metallic ferromagnets. *Nature Materials*, 15(5):501–506, feb 2016. 10.1038/nmat4593.

[43] R. Tomasello, E. Martinez, R. Zivieri, L. Torres, M. Carpentieri, and G. Finocchio. A strategy for the design of skyrmion racetrack memories. *Scientific Reports*, 4:6784, jan 2014. 10.1038/srep06784.

[44] M. Hervé, B. Dupé, R. Lopes, M. Böttcher, M. D. Martins, T. Balashov, L. Gerhard, J. Sinova, and W. Wulfhekel. Stabilizing spin spirals and isolated skyrmions at low magnetic field exploiting vanishing magnetic anisotropy. *Nature Communications*, 9(1):1015, dec 2018. 10.1038/s41467-018-03240-w.

[45] S. Heinze, K. von Bergmann, M. Menzel, J. Brede, A. Kubetzka, R. Wiesendanger, G. Bihlmayer, and S. Blügel. Spontaneous atomic-scale magnetic skyrmion lattice in two dimensions. *Nature Physics*, 7(9):713–718, sep 2011. 10.1038/nphys2045.

[46] O. Boulle, J. Vogel, H. Yang, S. Pizzini, D. de Souza Chaves, A. Locatelli, T. O. Menteş, A. Sala, L. D. Buda-Prejbeanu, O. Klein, M. Belmeguenai, Y. Roussigné, A. Stashkevich, S. M. Chérif, L. Aballe, M. Foerster, M. Chshiev, S. Auffret, I. M. Miron, and G. Gaudin. Room-temperature chiral magnetic skyrmions in ultrathin magnetic nanostructures. *Nature Nanotechnology*, 11(5):449–454, jan 2016. 10.1038/nnano.2015.315.

[47] A. Sonntag, J. Hermenau, S. Krause, and R. Wiesendanger. Thermal stability of an interface-stabilized skyrmion lattice. *Physical Review Letters*, 113(7):077202, aug 2014. 10.1103/PhysRevLett.113.077202.

[48] C. Moreau-Luchaire, C. Moutafis, N. Reyren, J. Sampaio, C. A. F. Vaz, N. Van Horne, K. Bouzehouane, K. Garcia, C. Deranlot, P. Warnicke, P. Wohlhüter, J.-M. George, M. Weigand, J. Raabe, V. Cros, and A. Fert. Additive interfacial chiral interaction in multilayers for stabilization of small individual skyrmions at room temperature. *Nature Nanotechnology*, 11:444–448, jan 2016. 10.1038/nnano.2015.313.

[49] A. Soumyanarayanan, N. Reyren, A. Fert, and C. Panagopoulos. Emergent phenomena induced by spin–orbit coupling at surfaces and interfaces. *Nature*, 539(7630):509–517, nov 2016. 10.1038/nature19820.

[50] E. Berganza, J. A. Fernandez-Roldan, M. Jaafar, A. Asenjo, K. Guslienko, and O. Chubykalo-Fesenko. 3d quasi-skyrmions in thick cylindrical and dome-shape soft nanodots. *Scientific Reports*, 12:1–9, 3 2022. 10.1038/s41598-022-07407-w.

[51] X. Zhang, Y. Zhou, K. M. Song, T. E. Park, J. Xia, M. Ezawa, X. Liu, W. Zhao, G. Zhao, and S. Woo. Skyrmion-electronics: writing, deleting, reading and processing magnetic skyrmions toward spintronic applications. *Journal of Physics: Condensed Matter*, 32:143001, 1 2020. 10.1088/1361-648X/AB5488.

[52] A. Aharoni. *Introduction to the theory of ferromagnetism*. Oxford University Press, 2000.

[53] W. F. Brown. *Micromagnetics*. New York: Wiley, 1963.

[54] A. Thiele. Steady-State Motion of Magnetic Domains. *Physical Review Letters*, 30(6):230–233, feb 1973. 10.1103/PhysRevLett.30.230.

[55] J. Sampaio, V. Cros, S. Rohart, A. Thiaville, and A. Fert. Nucleation, stability and current-induced motion of isolated magnetic skyrmions in nanostructures. *Nature Nanotechnology*, 8(3):839–844, oct 2013. 10.1038/nnano.2013.210.

[56] S. Finizio, K. Zeissler, S. Wintz, S. Mayr, T. Weßels, A. J. Huxtable, G. Burnell, C. H. Marrows, and J. Raabe. Deterministic field-free skyrmion nucleation at a nanoengineered injector device. *Nano Letters*, 19:7246–7255, 10 2019. 10.1021/acs.nanolett.9b02840.

[57] G. Finocchio, F. Büttner, R. Tomasello, M. Carpentieri, and M. Kläui. Magnetic skyrmions: from fundamental to applications. *Journal of Physics D: Applied Physics*, 49:423001, 9 2016. 10.1088/0022-3727/49/42/423001.

[58] F. Büttner, I. Lemesh, M. Schneider, B. Pfau, C. M. Günther, P. Hessing, J. Geilhufe, L. Caretta, D. Engel, B. Krüger, J. Viefhaus, S. Eisebitt, and G. S. D Beach. Field-free deterministic ultrafast creation of magnetic skyrmions by spin-orbit torques. *Nature Nanotechnology*, 12, 2017. 10.1038/NNANO.2017.178.

[59] R. Juge, K. Bairagi, K. G. Rana, J. Vogel, M. Sall, D. Mailly, V. T. Pham, Q. Zhang, N. Sisodia, M. Foerster, L. Aballe, M. Belmeguenai, Y. Roussigné, S. Auffret, L. D. Buda-Prejbeanu, G. Gaudin, D. Ravelosona, and O. Boulle. Helium ions put magnetic skyrmions on the track. *Nano Letters*, 21:2989–2996, 4 2021. 10.1021/acs.nanolett.1c00136.

[60] Y. Zhou, E. Iacocca, A. A. Awad, R. K. Dumas, F. C. Zhang, H. B. Braun, and J. Åkerman. Dynamically stabilized magnetic skyrmions. *Nature Communications*, 6:1–10, 9 2015. 10.1038/ncomms9193.

[61] F. Tejo, D. Toneto, S. Oyarzún, J. Hermosilla, C. S. Danna, J. L. Palma, R. B. D. Silva, L. S. Dorneles, and J. C. Denardin. Stabilization of magnetic skyrmions on arrays of self-assembled hexagonal nanodomes for magnetic recording applications. *ACS Applied Materials and Interfaces*, 12:53454–53461, 11 2020. 10.1021/acs.nanolett.1c00136.

[62] S. G. Je, D. Thian, X. Chen, L. Huang, D. H. Jung, W. Chao, K. S. Lee, J. I. Hong, A. Soumyanarayanan, and M. Y. Im. Targeted writing and deleting of magnetic skyrmions in two-terminal nanowire devices. *Nano Letters*, 21:1253–1259, 2 2021. 10.1021/acs.nanolett.0c03686.

[63] A. Casiraghi, H. Corte-León, M. Vafaee, F. Garcia-Sanchez, G. Durin, M. Pasquale, G. Jakob, M. Kläui, and O. Kazakova. Individual skyrmion manipulation by local magnetic field gradients. *Communications Physics*, 2:1–9, 11 2019. 10.1038/s42005-019-0242-5.

[64] V. M. Uzdin, M. N. Potkina, I. S. Lobanov, P. F. Bessarab, and H. Jónsson. Energy surface and lifetime of magnetic skyrmions. *Journal of Magnetism and Magnetic Materials*, 459:236–240, 8 2018. 10.1016/J.JMMM.2017.10.100.

[65] N. Del-Valle, S. Agramunt-Puig, A. Sanchez, and C. Navau. Imprinting skyrmions in thin films by ferromagnetic and superconducting templates. *Applied Physics Letters*, 107(13):133103, 2015. 10.1063/1.4932090.

[66] A. Siemens, Y. Zhang, J. Hagemeister, E. Y. Vedmedenko, and R. Wiesendanger. Minimal radius of magnetic skyrmions: statics and dynamics. *New Journal of Physics*, 18(4):045021, apr 2016. 10.1088/1367-2630/18/4/045021.

[67] S. Woo, K. M. Song, X. Zhang, Y. Zhou, M. Ezawa, X. Liu, S. Finizio, J. Raabe, N. J. Lee, S. I. Kim, S. Y. Park, Y. Kim, J. Y. Kim, D. Lee, O. Lee, J. W. Choi, B. C. Min, H. C. Koo, and J. Chang. Current-driven dynamics and inhibition of the skyrmion hall effect of ferrimagnetic skyrmions in gdfeco films. *Nature Communication*, 9:1–8, 3 2018. 10.1038/s41467-018-03378-7.

[68] N. S. Kiselev, A. N. Bogdanov, R. Schäfer, and U. K. Röler. Chiral skyrmions in thin magnetic films: new objects for magnetic storage technologies? *Journal of Physics D: Applied Physics*, 44:392001, 9 2011. 10.1088/0022-3727/44/39/392001.

[69] I. Purnama, W. L. Gan, D. W. Wong, and W. S. Lew. Guided current-induced skyrmion motion in 1D potential well. *Scientific Reports*, 5(1):10620, sep 2015. 10.1038/srep10620.

[70] S. Woo, K. M. Song, H. S. Han, M. S. Jung, M. Y. Im, K. S. Lee, K. S. Song, P. Fischer, J. I. Hong, J. W. Choi, B. C. Min, H. C. Koo, and J. Chang. Spin-orbit torque-driven skyrmion dynamics revealed by time-resolved x-ray microscopy. *Nature Communications*, 8:1–8, 5 2017.

[71] C. Navau, N. Del-Valle, and A. Sanchez. Analytical trajectories of skyrmions in confined geometries: Skyrmionic racetracks and nano-oscillators. *Physical Review B*, 94(18):184104, nov 2016. 10.1103/PhysRevB.94.184104.

[72] V. L. Carvalho-Santos, M. A. Castro, D. Salazar-Aravena, D. Laroze, R. M. Corona, S. Allende, and D. Altbir. Skyrmion propagation along curved racetracks. *Applied Physics Letters*, 118:172407, 4 2021. 10.1063/5.0045969.

[73] B. Göbel, A. Mook, J. Henk, and I. Mertig. Overcoming the speed limit in skyrmion racetrack devices by suppressing the skyrmion Hall effect. *Physical Review B*, 99(2):020405, jan 2019. 10.1103/PhysRevB.99.020405.

[74] J. Iwasaki, M. Mochizuki, and N. Nagaosa. Universal current-velocity relation of skyrmion motion in chiral magnets. *Nature Communications*, 4:1463, jan 2013. 10.1038/ncomms2442.

[75] C. Jin, C. Song, J. Wang, and Q. Liu. Dynamics of antiferromagnetic skyrmion driven by the spin Hall effect. *Applied Physics Letters*, 109(18):182404, oct 2016. 10.1063/1.4967006.

[76] S. K. Kim, K. J. Lee, and Y. Tserkovnyak. Self-focusing skyrmion racetracks in ferrimagnets. *Physical Review B*, 95(14):140404, apr 2017. 10.1103/PhysRevB.95.140404.

[77] X. Zhang, M. Ezawa, D. Xiao, G. P. Zhao, Y. Liu, and Y. Zhou. All-magnetic control of skyrmions in nanowires by a spin wave. *Nanotechnology*, 26(22):225701, jun 2015. 10.1088/0957-4484/26/22/225701.

[78] B. Zhang, W. Wang, M. Beg, H. Fangohr, and W. Kuch. Microwave-induced dynamic switching of magnetic skyrmion cores in nanodots. *Applied Physics Letters*, 106(10):102401, mar 2015. 10.1063/1.4914496.

[79] Y. Zhang, S. Luo, B. Yan, J. Ou-Yang, X. Yang, S. Chen, B. Zhu, and L. You. Magnetic skyrmions without the skyrmion Hall effect in a magnetic nanotrack with perpendicular anisotropy. *Nanoscale*, 9(29):10212–10218, jul 2017. 10.1039/C7NR01980G.

[80] P. Upadhyaya, G. Yu, P. K. Amiri, and K. L. Wang. Electric-field guiding of magnetic skyrmions. *Physical Review B*, 92(13):134411, oct 2015. 10.1103/PhysRevB.92.134411.

[81] D. Suess, C. Vogler, F. Bruckner, P. Heistracher, and C. Abert. A repulsive skyrmion chain as a guiding track for a racetrack memory. *AIP Advances*, 8:115301, 11 2018.

[82] S. Li, J. Xia, X. Zhang, M. Ezawa, W. Kang, X. Liu, Y. Zhou, and W. Zhao. Dynamics of a magnetic skyrmionium driven by spin waves. *Applied Physics Letters*, 112(14):142404, apr 2018. 10.1063/1.5026632.

[83] J. Müller. Magnetic skyrmions on a two-lane racetrack. *New Journal of Physics*, 19(2):025002, feb 2017. 10.1088/1367-2630/aa5b55.

[84] N. Del-Valle, J. Castell-Queralt, L. González-Gómez, and C. Navau. Defect modeling in skyrmionic ferromagnetic systems. *APL Materials*, 10(1):010702, jan 2022. 10.1063/5.0072709.

[85] C. Cheng, Z. Yan, J. Dong, Y. Liu, Z. Xia, L. Li, and X. Han. Elliptical skyrmion moving along a track without transverse speed. *Physical Review B*, 104:174409, 11 2021. 10.1103/PHYSREVB.104.174409/FIGURES/6/MEDIUM.

[86] C. Navau, N. Del-Valle, and A. Sanchez. Interaction of isolated skyrmions with point and linear defects. *Journal of Magnetism and Magnetic Materials*, 465:709–715, nov 2018. 10.1016/J.JMMM.2018.06.044.

[87] L. González-Gómez, J. Castell-Queralt, N. Del-Valle, A. Sanchez, and C. Navau. Analytical modeling of the interaction between skyrmions and extended defects. *Physical Review B*, 100(5):054440, aug 2019. 10.1103/PhysRevB.100.054440.

[88] H. C. Choi, S.-Z. Lin, and J.-X. Zhu. Density functional theory study of skyrmion pinning by atomic defects in MnSi. *Physical Review B*, 93(11):115112, mar 2016. 10.1103/PhysRevB.93.115112.

[89] C. Hanneken, A. Kubetzka, K. von Bergmann, and R. Wiesendanger. Pinning and movement of individual nanoscale magnetic skyrmions via defects. *New Journal of Physics*, 18(5):055009, may 2016. 10.1088/1367-2630/18/5/055009.

[90] I. Lima Fernandes, J. Bouaziz, S. Blügel, and S. Lounis. Universality of defect-skyrmion interaction profiles. *Nature Communications*, 9(1):4395, dec 2018. 10.1038/s41467-018-06827-5.

[91] D. Toscano, S. Leonel, P. Coura, and F. Sato. Building traps for skyrmions by the incorporation of magnetic defects into nanomagnets: Pinning and scattering traps by magnetic properties engineering. *Journal of Magnetism and Magnetic Materials*, 480:171–185, jun 2019. 10.1016/J.JMMM.2019.02.075.

[92] X. Chen, W. Kang, D. Zhu, X. Zhang, N. Lei, Y. Zhang, Y. Zhou, and W. Zhao. Skyrmion dynamics in width-varying nanotracks and implications for skyrmionic applications. *Applied Physics Letters*, 111(20):202406, nov 2017. 10.1063/1.5005953.

[93] X. Zhang, J. Xia, G. Zhao, X. Liu, and Y. Zhou. Magnetic Skyrmion Transport in a Nanotrack With Spatially Varying Damping and Non-adiabatic Torque. *IEEE Transactions on Magnetics*, pages 1–1, 2016. 10.1109/TMAG.2016.2641384.

[94] I. G. Arjana, I. L. Fernandes, J. Chico, and S. Lounis. Sub-nanoscale atom-by-atom crafting of skyrmion-defect interaction profiles. *Scientific Reports*, 10:1–12, 9 2020. 10.1038/s41598-020-71232-2.

[95] D. Stosic, T. B. Ludermir, and M. V. Milošević. Pinning of magnetic skyrmions in a monolayer Co film on Pt(111): Theoretical characterization and exemplified utilization. *Physical Review B*, 96(21):214403, dec 2017. 10.1103/PhysRevB.96.214403.

[96] J. Ding, X. Yang, and T. Zhu. Manipulating current induced motion of magnetic skyrmions in the magnetic nanotrack. *Journal of Physics D: Applied Physics*, 48:115004, 2 2015. 10.1088/0022-3727/48/11/115004.

[97] J. Mulkers, B. Van Waeyenberge, and M. V. Milošević. Effects of spatially engineered Dzyaloshinskii-Moriya interaction in ferromagnetic films. *Physical Review B*, 95(14):144401, apr 2017. 10.1103/PhysRevB.95.144401.

[98] A. Hrabec, N. A. Porter, A. Wells, M. J. Benitez, G. Burnell, S. McVitie, D. McGrouther, T. A. Moore, and C. H. Marrows. Measuring and tailoring the Dzyaloshinskii-Moriya interaction in perpendicularly magnetized thin films. *Physical Review B*, 90(2):020402, jul 2014. 10.1103/PhysRevB.90.020402.

[99] J. C. Martinez and M. B. A. Jalil. Topological dynamics and current-induced motion in a skyrmion lattice. *New Journal of Physics*, 18(3):033008, mar 2016. 10.1088/1367-2630/18/3/033008.

[100] I. Gross, W. Akhtar, A. Hrabec, J. Sampaio, L. J. Martínez, S. Chouaieb, B. J. Shields, P. Maletinsky, A. Thiaville, S. Rohart, and V. Jacques. Skyrmion morphology in ultrathin

magnetic films. *Physical Review Materials*, 2:024406, 2 2018. 10.1103/PHYSREVMATERIALS.2.024406/FIGURES/4/MEDIUM.

[101] A. Salimath, A. Abbout, A. Brataas, and A. Manchon. Current-driven skyrmion depinning in magnetic granular films. *Physical Review B*, 99(10):104416, mar 2019. 10.1103/PhysRevB.99.104416.

[102] J.-V. Kim and M.-W. Yoo. Current-driven skyrmion dynamics in disordered films. *Applied Physics Letters*, 110(13):132404, mar 2017. 10.1063/1.4979316.

[103] X. Gong, H. Y. Yuan, and X. R. Wang. Current-driven skyrmion motion in granular films. *Physical Review B*, 101:064421, Feb 2020. 10.1103/PhysRevB.101.064421.

[104] C. Reichhardt and C. J. Reichhardt. Nonlinear transport, dynamic ordering, and clustering for driven skyrmions on random pinning. *Physical Review B*, 99:104418, 3 2019. 10.1103/PhysRevB.99.104418.

[105] V. Raposo, R. F. Luis Martinez, and E. Martinez. Current-driven skyrmion motion along disordered magnetic tracks. *AIP Advances*, 7(5):056017, may 2017. 10.1063/1.4975658.

[106] W. Koshibae and N. Nagaosa. Theory of current-driven skyrmions in disordered magnets. *Scientific Reports*, 8:1–13, 4 2018. 10.1038/s41598-018-24693-5.

[107] C. Reichhardt, D. Ray, and C. J. O. Reichhardt. Collective Transport Properties of Driven Skyrmions with Random Disorder. *Physical Review Letters*, 114(21):217202, may 2015. 10.1103/PhysRevLett.114.217202.

[108] C. Reichhardt and C. J. Olson Reichhardt. Noise fluctuations and drive dependence of the skyrmion Hall effect in disordered systems. *New Journal of Physics*, 18(9):095005, sep 2016. 10.1088/1367-2630/18/9/095005.

[109] B. L. Brown, U. C. Täuber, and M. Pleimling. Skyrmion relaxation dynamics in the presence of quenched disorder. *Physical Review B*, 100:024410, 7 2019. 10.1103/PHYSREVB.100.024410/FIGURES/5/MEDIUM.

[110] S. A. Díaz, C. Reichhardt, D. P. Arovas, A. Saxena, and C. J. Reichhardt. Avalanches and criticality in driven magnetic skyrmions. *Physical Review Letters*, 120:117203, 3 2018. 10.1103/PhysRevLett.120.117203.

[111] X. Wang, W. L. Gan, J. C. Martinez, F. N. Tan, M. B. A. Jalil, and W. S. Lew. Efficient skyrmion transport mediated by a voltage controlled magnetic anisotropy gradient. *Nanoscale*, 10(2):733–740, jan 2018. 10.1039/C7NR06482A.

[112] B. W. Walker, C. Cui, F. Garcia-Sanchez, J. A. C. Incorvia, X. Hu, and J. S. Friedman. Skyrmion logic clocked via voltage-controlled magnetic anisotropy. *Applied Physics Letters*, 118:192404, 5 2021. 10.1063/5.0049024.

[113] X. Chen, W. Kang, D. Zhu, X. Zhang, N. Lei, Y. Zhang, Y. Zhou, and W. Zhao. Complementary Skyrmion Racetrack Memory Enables Voltage-Controlled Local Data Update Functionality. *IEEE Transactions on Electron Devices*, 65(10):4667–4673, oct 2018. 10.1109/TED.2018.2866912.

[114] W. Kang, Y. Huang, C. Zheng, W. Lv, N. Lei, Y. Zhang, X. Zhang, Y. Zhou, and W. Zhao. Voltage Controlled Magnetic Skyrmion Motion for Racetrack Memory. *Scientific Reports*, 6(1):23164, sep 2016. 10.1038/srep23164.

[115] R. Loreto, X. Zhang, Y. Zhou, M. Ezawa, X. Liu, and C. de Araujo. Manipulation of magnetic skyrmions in a locally modified synthetic antiferromagnetic racetrack. *Journal of Magnetism and Magnetic Materials*, 482:155–159, jul 2019. 10.1016/J.JMMM.2019.03.030.

[116] C. Song, C. Jin, J. Wang, H. Xia, J. Wang, and Q. Liu. Skyrmion-based multi-channel racetrack. *Applied Physics Letters*, 111(19):192413, nov 2017. 10.1063/1.4994093.

[117] X. Zhang, G. P. Zhao, H. Fangohr, J. P. Liu, W. X. Xia, J. Xia, and F. J. Morvan. Skyrmion-skyrmion and skyrmion-edge repulsions in skyrmion-based racetrack memory. *Scientific Reports*, 5:7643, jan 2015. 10.1038/srep07643.

[118] M. G. Morshed, H. Vakili, and A. W. Ghosh. Positional stability of skyrmions in a racetrack memory with notched geometry. *Physical Review Applied*, 17:064019, Jun 2022. 10.1103/PhysRevApplied.17.064019.

[119] J. J. Liang, J. H. Yu, and J. Chen. Manipulating and trapping skyrmions by magnetic field gradients Related content Magnetic field gradient driven dynamics of isolated skyrmions and antiskyrmions in frustrated magnets. 2017. 10.1088/1367-2630/aa7812.

[120] J. J. Liang, J. H. Yu, J. Chen, M. H. Qin, M. Zeng, X. B. Lu, X. S. Gao, and J. M. Liu. Magnetic field gradient driven dynamics of isolated skyrmions and antiskyrmions in frustrated magnets. *New Journal of Physics*, 20:053037, 5 2018. 10.1088/1367-2630/AAC24C.

[121] S. L. Zhang, W. W. Wang, D. M. Burn, H. Peng, H. Berger, A. Bauer, C. Pfleiderer, G. van der Laan, and T. Hesjedal. Manipulation of skyrmion motion by magnetic field gradients. *Nature Communications*, 9(1):2115, dec 2018. 10.1038/s41467-018-04563-4.

[122] R. Khoshlahni, A. Qaiumzadeh, A. Bergman, and A. Brataas. Ultrafast generation and dynamics of isolated skyrmions in antiferromagnetic insulators. *Physical Review B*, 99:054423, Feb 2019.

[123] L. Kong and J. Zang. Dynamics of an Insulating Skyrmion under a Temperature Gradient. *Physical Review Letters*, 111(6):067203, aug 2013. 10.1103/PhysRevLett.111.067203.

[124] K. Everschor, M. Garst, B. Binz, F. Jonietz, S. Mühlbauer, C. Pfleiderer, and A. Rosch. Rotating skyrmion lattices by spin torques and field or temperature gradients. *Physical Review B*, 86(5):054432, aug 2012. 10.1103/PhysRevB.86.054432.

[125] L. González-Gómez, J. Castell-Queralt, N. Del-Valle, and C. Navau. Mutual interaction between superconductors and ferromagnetic skyrmionic structures in confined geometries. *Physical Review Applied*, 17:034069, 3 2022. 10.1103/PHYSREVAPPLIED.17.034069/FIGURES/6/MEDIUM.

[126] S. Luo, M. Song, X. Li, Y. Zhang, J. Hong, X. Yang, X. Zou, N. Xu, and L. You. Reconfigurable skyrmion logic gates. *Nano Letters*, 18:1180–1184, 2 2018.

[127] M. Chauwin, X. Hu, F. Garcia-Sanchez, N. Betrabet, A. Paler, C. Moutafis, and J. S. Friedman. Skyrmion logic system for large-scale reversible computation. *Physical Review Applied*, 12:064053, 12 2019.

[128] M. Song, M. G. Park, S. Ko, S. K. Jang, M. Je, and K. J. Kim. Logic device based on skyrmion annihilation. *IEEE Transactions on Electron Devices*, 68:1939–1943, 4 2021. 10.1109/TED.2021.3055157.

[129] X. Zhang, Y. Zhou, M. Ezawa, G. P. Zhao, and W. Zhao. Magnetic skyrmion transistor: skyrmion motion in a voltage-gated nanotrack. *Scientific Reports*, 5:11369, jan 2015. 10.1038/srep11369.

[130] L. Zhao, Z. Wang, X. Zhang, X. Liang, J. Xia, K. Wu, H. A. Zhou, Y. Dong, G. Yu, K. L. Wang, X. Liu, Y. Zhou, and W. Jiang. Topology-Dependent Brownian Gyromotion of a Single Skyrmion. *Physical Review Letters*, 125(2):027206, jul 2020. 10.1103/PHYSREVLETT.125.027206/FIGURES/4/MEDIUM.

[131] L. Zhao, Z. Wang, X. Zhang, X. Liang, J. Xia, K. Wu, H.-A. Zhou, Y. Dong, G. Yu, K. L. Wang, X. Liu, Y. Zhou, and W. Jiang. Topology-dependent brownian gyromotion of a single skyrmion. *Physical Review Letters*, 125:027206, Jul 2020. 10.1103/PhysRevLett.125.027206.

[132] J. Miltat, S. Rohart, and A. Thiaville. Brownian motion of magnetic domain walls and skyrmions, and their diffusion constants. *Physical Review B*, 97(21):214426, jun 2018. 10.1103/PhysRevB.97.214426.

[133] X. Zhang, M. Ezawa, and Y. Zhou. Thermally stable magnetic skyrmions in multilayer synthetic antiferromagnetic racetracks. *Physical Review B*, 94(6):064406, aug 2016. 10.1103/PhysRevB.94.064406.

[134] P. F. Bessarab, G. P. Müller, I. S. Lobanov, F. N. Rybakov, N. S. Kiselev, H. Jónsson, V. M. Uzdin, S. Blügel, L. Bergqvist, and A. Delin. Lifetime of racetrack skyrmions. *Scientific Reports*, 8(1):3433, dec 2018. 10.1038/s41598-018-21623-3.

[135] I. Medlej, A. Hamadeh, and F. E. H. Hassan. Skyrmion based random bit generator. *Physica B: Condensed Matter*, 579:411900, feb 2020. 10.1016/J.PHYSB.2019.411900.

[136] C. T. Ma, Y. Xie, H. Sheng, A. W. Ghosh, and S. J. Poon. Robust formation of ultrasmall room-temperature neél skyrmions in amorphous ferrimagnets from atomistic simulations. *Scientific Reports*, 9:1–10, 7 2019. 10.1038/s41598-019-46458-4.

[137] K. Litzius, J. Leliaert, P. Bassirian, D. Rodrigues, S. Kromin, I. Lemesh, J. Zazvorka, K. J. Lee, J. Mulkers, N. Kerber, D. Heinze, N. Keil, R. M. Reeve, M. Weigand, B. V. Waeyenberge, G. Schütz, K. Everschor-Sitte, G. S. Beach, and M. Kläui. The role of temperature and drive current in skyrmion dynamics. *Nature Electronics*, 3:30–36, 1 2020. 10.1038/s41928-019-0359-2.

[138] C. Navau and J. Sort. Exploiting random phenomena in magnetic materials for data security, logics, and neuromorphic computing: Challenges and prospects. *APL Materials*, 9:070903, 7 2021. 10.1063/5.0055400.

[139] L. Exl, D. Suess, and T. Schrefl. Micromagnetism. *Handbook of Magnetism and Magnetic Materials*, pages 1–44, 2021. 10.1007/978-3-030-63101-7_7 − 1.

[140] L. D. Landau and E. Lifshitz. On the theory of the dispersion of magnetic permeability in ferromagnetic bodies. *Phys. Z. Sowjet.*, 8:153, 1935.

[141] T. Gilbert. Classics in Magnetics A Phenomenological Theory of Damping in Ferromagnetic Materials. *IEEE Transactions on Magnetics*, 40(6):3443–3449, nov 2004. 10.1109/TMAG.2004.836740.

[142] M. Lakshmanan. The fascinating world of the landaulifshitzgilbert equation: an overview. *Philosophical Transactions of the Royal Society A: Mathematical, Physical and Engineering Sciences*, 369:1280–1300, 3 2011. 10.1098/RSTA.2010.0319.

[143] L. Ranno and M. A. Moro. Design Rules for DMI-Stabilised Skyrmions, 2021. 10.48550/ARXIV.2107.00767. `https://arxiv.org/abs/2107.00767`.

[144] J. M. D. Coey. *Magnetism and Magnetic Materials*. Cambridge University Press, Cambridge, 2010. 10.1017/CBO9780511845000.

[145] C. Kittel, by C Zener, J. C. Slater, E. P. Wohlfarth, J. H. V. V. A, and R. R. Heikes. Symposium on exchange. *Review of modernphysics*, 25, 1953.

[146] C. Kittel. Indirect exchange interactions in metals. *Solid State Physics - Advances in Research and Applications*, 22:1–26, 1 1969. 10.1016/S0081-1947(08)60030-2.

[147] A. R. Biedermann. Magnetic anisotropy in single crystals: A review. *Geosciences*, 8:302, 8 2018. 10.3390/GEOSCIENCES8080302.

[148] J. Slonczewski. Current-driven excitation of magnetic multilayers. *Journal of Magnetism and Magnetic Materials*, 159(1-2):L1–L7, jun 1996. 10.1016/0304-8853(96)00062-5.

[149] Z. Li and S. Zhang. Domain-Wall Dynamics and Spin-Wave Excitations with Spin-Transfer Torques. *Physical Review Letters*, 92(20):207203, may 2004. 10.1103/PhysRevLett.92.207203.

[150] S. Zhang and Z. Li. Roles of Nonequilibrium Conduction Electrons on the Magnetization Dynamics of Ferromagnets. *Physical Review Letters*, 93(12):127204, sep 2004. 10.1103/PhysRevLett.93.127204.

[151] Y. B. Bazaliy, B. A. Jones, and S.-C. Zhang. Modification of the Landau-Lifshitz equation in the presence of a spin-polarized current in colossal- and giant-magnetoresistive materials. *Physical Review B*, 57(6):R3213–R3216, feb 1998. 10.1103/PhysRevB.57.R3213.

[152] S. Emori, U. Bauer, S.-M. Ahn, E. Martinez, and G. S. D. Beach. Current-driven dynamics of chiral ferromagnetic domain walls. *Nature Materials*, 12(7):611–616, jul 2013. 10.1038/nmat3675.

[153] L. Liu, O. J. Lee, T. J. Gudmundsen, D. C. Ralph, and R. A. Buhrman. Current-Induced Switching of Perpendicularly Magnetized Magnetic Layers Using Spin Torque from the Spin Hall Effect. *Physical Review Letters*, 109(9):096602, aug 2012. 10.1103/PhysRevLett.109.096602.

[154] R. Tomasello, A. Giordano, S. Chiappini, R. Zivieri, G. Siracusano, V. Puliafito, I. Medlej, A. La Corte, B. Azzerboni, M. Carpentieri, Z. Zeng, and G. Finocchio. Micromagnetic understanding of the skyrmion hall angle current dependence in perpendicularly magnetized ferromagnets. *Physical Review B*, 98(22):224418, dec 2018. 10.1103/PhysRevB.98.224418.

[155] S. Rohart and A. Thiaville. Skyrmion confinement in ultrathin film nanostructures in the presence of Dzyaloshinskii-Moriya interaction. *Physical Review B*, 88(18):184422, nov 2013. 10.1103/PhysRevB.88.184422.

[156] A. Vansteenkiste, J. Leliaert, M. Dvornik, M. Helsen, F. Garcia-Sanchez, and B. Van Waeyenberge. The design and verification of mumax3. *AIP Advances*, 4(10):107133, 2014. 10.1063/1.4899186.

[157] M. Donahue. Oommf user's guide, version 1.0, 1999-09-01 1999. https://doi.org/10.6028/NIST.IR.6376. `https://nvlpubs.nist.gov/nistpubs/Legacy/IR/nistir6376.pdf`.

[158] T. Schulz, R. Ritz, A. Bauer, M. Halder, M. Wagner, C. Franz, C. Pfleiderer, K. Everschor, M. Garst, and A. Rosch. Emergent electrodynamics of skyrmions in a chiral magnet. *Nature Physics*, 8(4):301–304, apr 2012. 10.1038/nphys2231.

[159] K. Litzius, I. Lemesh, B. Krüger, P. Bassirian, L. Caretta, K. Richter, F. Büttner, K. Sato, O. A. Tretiakov, J. Förster, R. M. Reeve, M. Weigand, I. Bykova, H. Stoll, G. Schütz, G. S. D. Beach, and M. Kläui. Skyrmion Hall effect revealed by direct time-resolved X-ray microscopy. *Nature Physics*, 13(2):170–175, dec 2016. 10.1038/nphys4000.

[160] W. Legrand, D. Maccariello, N. Reyren, K. Garcia, C. Moutafis, C. Moreau-Luchaire, S. Collin, K. Bouzehouane, V. Cros, and A. Fert. Room-Temperature Current-Induced Generation and Motion of sub-100 nm Skyrmions. *Nano Letters*, 17(4):2703–2712, apr 2017. 10.1021/acs.nanolett.7b00649.

[161] W. Jiang, X. Zhang, G. Yu, W. Zhang, X. Wang, M. Benjamin Jungfleisch, J. E. Pearson, X. Cheng, O. Heinonen, K. L. Wang, Y. Zhou, A. Hoffmann, S. te Velthuis, and G. E. Direct observation of the skyrmion Hall effect. *Nature Physics*, 13(2):162–169, sep 2016. 10.1038/nphys3883.

[162] J. Iwasaki, W. Koshibae, and N. Nagaosa. Colossal Spin Transfer Torque Effect on Skyrmion along the Edge. *Nano Letters*, 14(8):4432–4437, aug 2014. 10.1021/nl501379k.

[163] N. Romming, C. Hanneken, M. Menzel, J. E. Bickel, B. Wolter, K. von Bergmann, A. Kubetzka, and R. Wiesendanger. Writing and deleting single magnetic skyrmions. *Science (New York, N.Y.)*, 341(6146):636–9, aug 2013. 10.1126/science.1240573.

[164] A. S. Varentcova, S. von Malottki, M. N. Potkina, G. Kwiatkowski, S. Heinze, and P. F. Bessarab. Toward room-temperature nanoscale skyrmions in ultrathin films. *Computational Materials*, 6:1–11, 12 2020. 10.1038/s41524-020-00453-w.

[165] X. Z. Yu, W. Koshibae, Y. Tokunaga, K. Shibata, Y. Taguchi, N. Nagaosa, and Y. Tokura. Transformation between meron and skyrmion topological spin textures in a chiral magnet. *Nature*, 564:95–98, 12 2018. 10.1038/s41586-018-0745-3.

[166] T. Matsumoto, Y.-G. So, Y. Kohno, Y. Ikuhara, N. Shibata, and J. Limited. Stable magnetic skyrmion states at room temperature confined to corrals of artificial surface pits fabricated by a focused electron beam. 2018. 10.1021/acs.nanolett.7b03967.

[167] N. Nagaosa and Y. Tokura. Topological properties and dynamics of magnetic skyrmions. *Nature Nanotechnology*, 8(12):899–911, dec 2013. 10.1038/nnano.2013.243.

[168] A. Neubauer, C. Pfleiderer, B. Binz, A. Rosch, R. Ritz, P. G. Niklowitz, and P. Böni. Topological hall effect in the a phase of mnsi. *Physical Review Letters*, 102:186602, 5 2009. 10.1103/PHYSREVLETT.102.186602/FIGURES/4/MEDIUM.

[169] J. Zang, M. Mostovoy, J. H. Han, and N. Nagaosa. Dynamics of skyrmion crystals in metallic thin films. *Physical Review Letters*, 107:136804, 9 2011. 10.1103/PhysRevLett.107.136804.

[170] W. Jiang, G. Chen, K. Liu, J. Zang, S. G. te Velthuis, and A. Hoffmann. Skyrmions in magnetic multilayers. *Physics Reports*, 704:1–49, aug 2017. 10.1016/J.PHYSREP.2017.08.001.

[171] C. Reichhardt, D. Ray, and C. O. Reichhardt. Collective Transport Properties of Driven Skyrmions with Random Disorder. *Physical Review Letters*, 114(21):217202, may 2015. 10.1103/PhysRevLett.114.217202.

[172] C. Reichhardt, D. Ray, and C. J. O. Reichhardt. Quantized transport for a skyrmion moving on a two-dimensional periodic substrate. *Physical Review B*, 91(10):104426, mar 2015. 10.1103/PhysRevB.91.104426.

[173] C. Reichhardt and C. J. O. Reichhardt. Nonlinear Transport, Dynamic Ordering, and Clustering for Driven Skyrmions on Random Pinning. aug 2018.

[174] J. Müller and A. Rosch. Capturing of a magnetic skyrmion with a hole. *Physical Review B*, 91(5):054410, feb 2015. 10.1103/PhysRevB.91.054410.

[175] S. Panigrahy, S. Mallick, J. Sampaio, and S. Rohart. Skyrmion inertia in synthetic antiferromagnets. *Physical Review B*, 106:144405, 10 2022. 10.1103/PHYSREVB.106.144405/FIGURES/5/MEDIUM.

[176] J. Iwasaki, M. Mochizuki, and N. Nagaosa. Current-induced skyrmion dynamics in constricted geometries. *Nature Nanotechnology*, 8(10):742–7, oct 2013. 10.1038/nnano.2013.176.

[177] S. Komineas and N. Papanicolaou. Skyrmion dynamics in chiral ferromagnets. *Physical Review B*, 92(6):064412, aug 2015. 10.1103/PhysRevB.92.064412.

[178] S. Rohart, J. Miltat, and A. Thiaville. Path to collapse for an isolated Néel skyrmion. *Physical Review B*, 93(21):214412, jun 2016. 10.1103/PhysRevB.93.214412.

[179] S. Luo, Y. Zhang, M. Shen, J. Ou-Yang, B. Yan, X. Yang, S. Chen, B. Zhu, and L. You. Skyrmion-based high-frequency signal generator. *Applied Physics Letters*, 110(11):112402, mar 2017. 10.1063/1.4978510.

[180] J. Müller, A. Rosch, and M. Garst. Edge instabilities and skyrmion creation in magnetic layers. *New Journal of Physics*, 18(6):065006, jun 2016. 10.1088/1367-2630/18/6/065006.

[181] A. O. Leonov and M. Mostovoy. Edge states and skyrmion dynamics in nanostripes of frustrated magnets. *Nature Communications*, 8:14394, feb 2017. 10.1038/ncomms14394.

[182] X. Zhang, Y. Zhou, and M. Ezawa. Magnetic bilayer-skyrmions without skyrmion Hall effect. *Nature Communications*, 7:10293, jan 2016. 10.1038/ncomms10293.

[183] K. M. Song, J. S. Jeong, B. Pan, X. Zhang, J. Xia, S. Cha, T. E. Park, K. Kim, S. Finizio, J. Raabe, J. Chang, Y. Zhou, W. Zhao, W. Kang, H. Ju, and S. Woo. Skyrmion-based artificial synapses for neuromorphic computing. *Nature Electronics*, 3:148–155, 3 2020. 10.1038/s41928-020-0385-0.

[184] Z. Yu, M. Shen, Z. Zeng, S. Liang, Y. Liu, M. Chen, Z. Zhang, Z. Lu, L. You, X. Yang, Y. Zhang, and R. Xiong. Voltage-controlled skyrmion-based nanodevices for neuromorphic computing using a synthetic antiferromagnet. *Nanoscale Advances*, 2:1309–1317, 3 2020. 10.1039/D0NA00009D.

[185] S. Luo and L. You. Skyrmion devices for memory and logic applications. *APL Materials*, 9:050901, 5 2021. 10.1063/5.0042917.

[186] S. Huang, C. Zhou, G. Chen, H. Shen, A. K. Schmid, K. Liu, and Y. Wu. Stabilization and current-induced motion of antiskyrmion in the presence of anisotropic Dzyaloshinskii-Moriya interaction. *Physical Review B*, 96(14):144412, oct 2017. 10.1103/PhysRevB.96.144412.

[187] M. Weißenhofer, L. Rózsa, and U. Nowak. Skyrmion dynamics at finite temperatures: Beyond thiele's equation. *Physical Review Letters*, 127:047203, 7 2021. 10.1103/PHYSREVLETT.127.047203/FIGURES/4/MEDIUM.

II - PAPERS

PAPER A

Exploiting symmetries in skyrmionic micromagnetic simulations: Cylindrical and radial meshes.

Castell-Queralt, Josep; Gonzalez-Gomez, Leonardo Gastón; Del-Valle, Nuria; Navau, Carles.

Journal of Magnetism and Magnetic Materials, Vol. 549, 168972, p. 1-7.

DOI: https://doi.org/10.1016/j.jmmm.2021.168972

PAPER B

Accelerating, guiding, and compressing skyrmions by defect rails

Castell-Queralt, Josep; Gonzalez-Gomez, Leonardo Gastón; Del-Valle, Nuria; Sanchez, Alvaro; Navau, Carles.

Nanoscale, Vol. 11, p. 12589-12594

DOI: https://doi-org.are.uab.cat/10.1039/C9NR02171J

PAPER C

Deterministic approach to skyrmionic dynamics at nonzero temperatures: Pinning sites and racetracks.

Castell-Queralt, Josep; Gonzalez-Gomez, Leonardo Gastón; Del-Valle, Nuria; Navau, Carles.

Physical Review B, Vol. 101, 140404, 30.03.2020.

DOI: https://doi.org/10.1103/PhysRevB.101.140404

PAPER D

Survival of skyrmions along granular racetracks at room temperature

Castell-Queralt, Josep; Gonzalez-Gomez, Leonardo Gastón; Del-Valle, Nuria; Navau, Carles.

Survival of skyrmions along granular racetracks at room temperature

Josep Castell-Queralt, Guillermo Abad-López, Leonardo González-Gómez, Nuria Del-Valle, and Carles Navau*

Departament de Física, Universitat Autònoma de Barcelona, 08193 Bellaterra, Barcelona, Catalonia, Spain

E-mail: carles.navau@uab.cat

Abstract

Skyrmions can be envisioned as bits of information that can be transported along nanoracetracks. However, temperature, defects, and/or granularity can produce diffusion, pinning, and, in general, modification in their dynamics. These effects may cause undesired errors in information transport. We present simulations of a realistic system where both the (room) temperature and sample granularity are taken into account. Key feasibility magnitudes, such as the success probability of a skyrmion traveling a given distance along the racetrack, are calculated. The results are evaluated in terms of the eventual loss of skyrmions by pinning, destruction at the edges, or excessive delay due to granularity. The model proposed is based on the Fokker-Planck equation resulting from the Thiele's rigid model for skyrmions. The results could serve to establish error detection criteria and, in general, to discern the dynamics of skyrmions in realistic situations.

Magnetic skyrmions are whirling magnetic structures that can be found in certain magnetic materials.[1] Their small size and high mobility have promoted them as promising information carriers, as well as building blocks in ultradense magnetic memories, logic devices, and

computational systems.[2–6] In ferromagnetic ultrathin films, with a heavy-metal substrate, it has been found that skyrmions can be stabilised with the aid of interfacial Dzyaloshinskii-Moriya interaction.[7–10] The same mechanism allows the formation of skyrmions in multilayers with alternating ferromagnets (FMs) and heavy-metals.[11,12] The experimental finding of room-temperature skyrmions[13] has boosted the potentiality of skyrmions for applications and, consequently, the study of their spin-current driven dynamics at non-zero temperatures to predict the feasibility of the aforementioned applications.

One of the most promising skyrmion-based applications proposed up to date is the skyrmionic racetrack memory. It is designed to drive skyrmions along the racetrack, with the spin-orbit torque produced by a spin-polarized current fed into a heavy-metal substrate.[2,14] In such systems, the borders of the track create a confining potential that sets a driving velocity upper threshold above which the skyrmions would escape the track.[15–18] Hence, when transporting stable skyrmions at zero temperature along a clean (defect-free and grain-free) racetrack we have two possible scenarios depending on the driving current: either the skyrmion is annihilated at the edge or it is channeled along the racetrack.

However, real skyrmionic racetracks are granular, and one would like to operate at room temperature. It is known that granularity acts as an array of pinning potentials for skyrmions that results in a minimum applied current density for the activation of skyrmion motion.[19–24] At room temperature, stochastic effects on the skyrmions position[25–27] could compromise their stability when approaching the borders or defects.[16,28] Moreover, even above the minimum threshold, there is a certain probability of being trapped.[29,30]

As a consequence, in a real racetrack, there is no longer a binary scenario for the survival of skyrmions. The problem becomes probabilistic. Here we address this problem by realistically simulating a nanoracetrack for skyrmions transport, taking into account both the (room) temperature and granularity. We use a deterministic, yet probabilistic, approach to study the dynamics of a skyrmion in a granular racetrack at room temperature. In the present work, we first model the interaction of the grains of the system with a skyrmion and

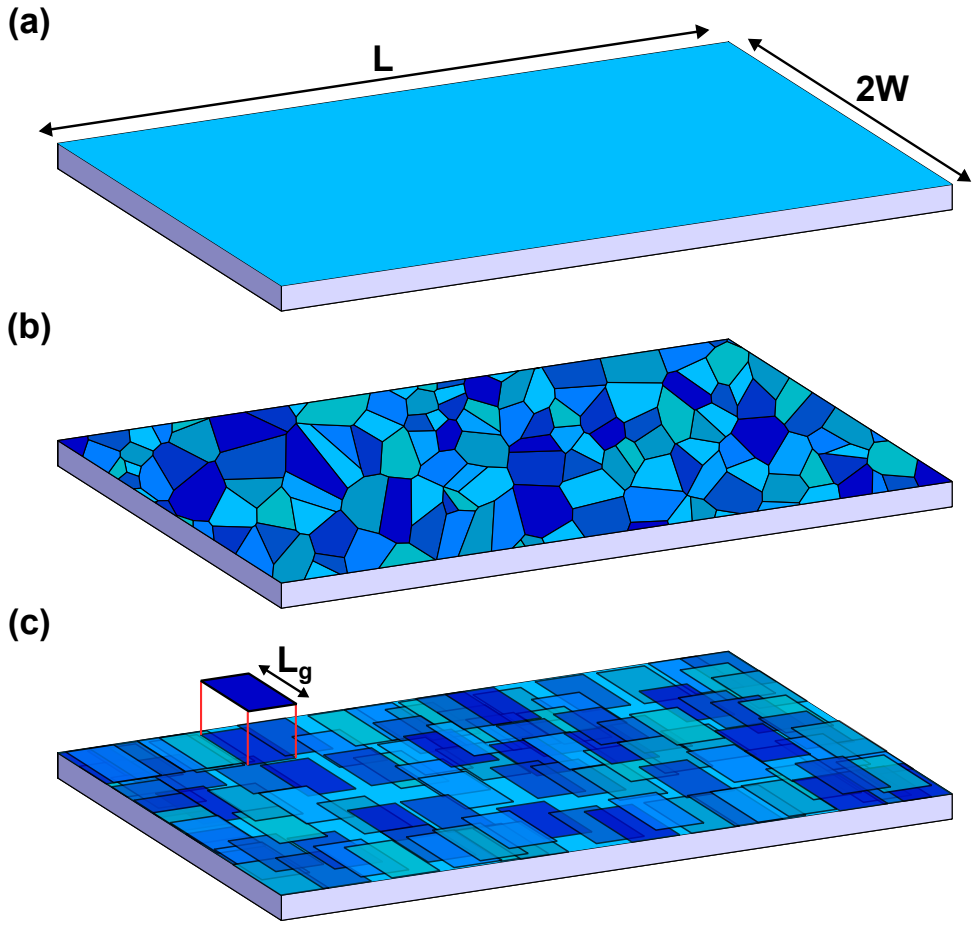

Figure 1: Sketch of the modeled racetrack. (a) Clean racetrack: the skyrmion is driven along the track of length L and confined by the borders at $y = \pm W$. (b) A Voronoi tessellation showing a possible grain structure. (c) The grains are modeled as square regions randomly distributed in the plane with Gaussian distributed anisotropy constants (represented by the different blue tones in the sketch).

derive the stochastic Thiele's equation (STE); second, we obtain the corresponding Fokker-Planck equation (FPE), which includes the temperature, and solve it numerically; and third, we study the feasibility of skyrmionic racetracks and how granularity affects the performance of such devices at room temperature.

The rigid (Thiele's) model[31] assumes that, during motion, the internal structure of the skyrmion is not modified, so its position and velocity can be described by generalized magnitudes, $\mathbf{r}_s$ and $\mathbf{v}_s$ respectively. We consider that the skyrmion is moving along a thin ferromagnetic racetrack of length L and width $2W$. The thickness of the ferromagnetic layer

is $d \ll W, L$. Thus, the magnetization is considered uniform across the thickness and we locate the FM layer at $z = 0$ (see sketch in Fig. 1a). Considering symmetric Néel-type skyrmions on a background magnetization pointing to $-\hat{\mathbf{z}}$, the STE for the movement of skyrmions driven by damping-like torques (produced by spin-polarized currents arising from the spin-Hall effect) after feeding an in-plane current $\mathbf{J}_H$ in a heavy-metal substrate, is[32,33]

$$(\mathbb{G} - M_s\alpha\mathbb{D})\mathbf{v}_s + M_s\mathbb{N}\mathbf{v}_H + \gamma M_s^2(\mathbf{F}_{\text{ext}} + \mathbf{F}_{\text{st}}) = 0, \tag{1}$$

where $\mathbb{G} = \begin{pmatrix} 0 & G \\ -G & 0 \end{pmatrix}$, $\mathbb{D} = \begin{pmatrix} D & 0 \\ 0 & D \end{pmatrix}$, and $\mathbb{N} = \begin{pmatrix} 0 & -N \\ N & 0 \end{pmatrix}$, being G, D, and N constants that depend on the internal structure of the skyrmion. α is the Gilbert damping constant, γ ($\gamma = 2.21 \cdot 10^5$ m A^{-1} s^{-1}) the gyromagnetic constant, $\mathbf{v}_H = -\frac{\mu_B\theta_H}{eM_s}(\hat{\mathbf{z}} \times \mathbf{J}_H)$, being μ_B the Bohr magneton, θ_H the Hall angle, e (> 0) the charge of the electron, and M_s the saturation magnetization. We use $G = 4\pi d M_s^3$, $D = 4\pi d M_s^2$ and $N = 4\pi R M_s^2$, where R is the radius of the rigid skyrmion. These values correspond to ideal Néel skyrmions with z-magnetization $M_z = M_s(R^2 - \rho^2)/(\rho^2 + R^2)$. $\mathbf{F}_{\text{st}}$ and $\mathbf{F}_{\text{ext}}$ come from the stochastic and external forces, respectively. They will contain the information about the temperature and granularity, as explained below.

On the one hand, the temperature T is introduced by considering the term $\mathbf{F}_{\text{st}}$ a white noise with $\langle F_{\text{st},j}\rangle = 0$ and $\langle F_{\text{st},i}\,,\, F_{\text{st},j}\rangle = \frac{2\alpha D k_B T}{\gamma\mu_0 M_s}\delta_{ij}\delta(t - t')$, being $i, j = x, y, z$. μ_0 is the vacuum permeability, k_B the Boltzmann constant, δ_{ij} the Kronecker delta and $\delta(t - t')$ the temporal Dirac's delta.[25]

On the other hand, $\mathbf{F}_{\text{ext}}$ has two contributions, $\mathbf{F}_{\text{ext}} = \mathbf{F}_R + \mathbf{F}_G$. The force[1] coming from the confining potential of the racetrack is $\mathbf{F}_R$ and the force produced by the granularity is $\mathbf{F}_G$.

The edges of a racetrack create a confining potential that repels the skyrmion. However,

[1]Strictly, $\mathbf{F}_{\text{ext}}$ and $\mathbf{F}_{\text{st}}$ do not have units of force. Nevertheless, we call them "force terms", following the usual nomenclature.

if a large enough driving current is applied, this potential can be overcome and the skyrmion is annihilated when it reaches the edge. An exponential function decaying with the edge-skyrmion distance has been proposed to account for these facts.[15,34] Thus, the force created by the borders of the racetrack over a skyrmion, whose generalized position is $\mathbf{r}_s = x_s\hat{\mathbf{x}} + y_s\hat{\mathbf{y}}$, is modeled as

$$\mathbf{F}_R = f_0 \left[e^{-(y_s+W)/R} - e^{-(y_s-W)/R} \right] \hat{\mathbf{y}}, \tag{2}$$

where f_0 is a parameter that controls the strength of the repulsion.

Since the rigid model does not allow to consider the skyrmion deformation near the edges, we also assume that a skyrmion is annihilated when it "touches" any racetrack border. That is, when the distance between its center and the edge equals the radius of the skyrmion.

To model the granularity force term, $\mathbf{F}_G$, is a more intrincated task. The physical origin of this term arises from the different physical properties values of the different grains that form the FM films. Despite all the relevant magnetic parameters can vary slightly between grains (e.g., exchange constant, Dzyaloshinskii-Moriya constant, or M_s) the most (usually) modified one is the uniaxial anisotropy constant, as the strength and the direction of the uniaxial anisotropy strongly depends on the crystalographic orientation of the material.[23,35] For simplicity, we only consider variations of anisotropy in our model.

A common approach to model granularity within the micromagnetic model is to generate a random set of grains, using Voronoi tessellation,[30,36,37] with an average size and some randomly distributed variation of anisotropy constant in each grain (see Fig. 1b). However, there is no clear way of how to translate this into the rigid model.

Here we use a slightly different approach. In Ref. [38], an analytical expression for the Thiele's force term generated by a single atomic defect that consist of a local modification of anisotropy, $\mathbf{F}_{\mathrm{ld}}$, was found as

$$\mathbf{F}_{\mathrm{ld}} = \frac{Ka^2\gamma}{\mu_0 M_s} \frac{4\,\Delta K\, R^2 r(R^2 - r^2)}{(R^2 + r^2)^3}\, \hat{\mathbf{r}}, \tag{3}$$

where K is the value of the anisotropy constant of the plain sample and ΔK the variation of the defect anisotropy with respect to K. a is the lattice constant and r is the distance from the position of (the center of) the skyrmion to the defect.

We consider each grain as a surface with an atomic defect density given by $\sigma_{\rm ld} = 1/a^2$. Each surface differential $\mathrm{d}S$ generates a differential of force given by $\sigma_{\rm ld}\mathbf{F}_{\rm ld}\,\mathrm{d}S$. Then, the force that a grain exerts over a skyrmion is

$$\mathbf{F}_{\rm gr} = \int_{S_g} \sigma_{\rm ld}\,\mathbf{F}_{\rm ld}\,\mathrm{d}S, \tag{4}$$

where the integration is done over the grain surface, S_g.

The problem now is that the position and shape of the grains have to be known in order to evaluate this force term. The grain distribution is modeled as follows. Consider that the whole surface of the track (of total surface area $2WL$) is formed by N_g grains of square shape and surface area L_g^2. Thus, $N_g = 2WL/L_g^2$. Those grains are randomly distributed over the track with the constraint that there cannot be more than four grain centers in any given square surface of side L_g (see Fig. 1c).

The typical size of grains is $L_g \simeq 10 - 20$ nm while the radius of skyrmions with the parameters used here (see below) is $R \simeq 80$ nm. Thus, when evaluating the force over a skyrmion due to a given grain its relative orientation with respect to the skyrmion and its shape are not relevant. $\mathbf{F}_{\rm gr}$ can be thus evaluated as

$$\mathbf{F}_{\rm gr} = f_G \left[\arctan\left(\frac{L_g/2}{r_0}\right)\left(\frac{-2}{r_0} + \frac{R^2}{r_0^3}\right) + \frac{R^2 L_g}{2r_0^2[(L_g/2)^2 + r_0^2]} \right]_{r_-}^{r_+} \hat{\mathbf{r}}. \tag{5}$$

Equation (5) is found after Eq. (4), by arbitrarily choosing that the line segment that goes from the center of the grain to the skyrmion position crosses perpendicularly one of the sides of the grain. We have checked that considering other orientations and shapes the difference in the force is less than 6%. The constant f_G is $f_G = (2K\Delta K\gamma R^2)/(\mu_0 M_s)$. The variable r_0 should be evaluated at $r_\pm = \sqrt{(r \pm L_g/2)^2 + R^2}$. r is now the distance between the grain

center and the position of the skyrmion.

Finally, the total force over a skyrmion is the sum over all the grains,

$$\mathbf{F}_G = \sum_{i=1}^{N_g} |\mathbf{F}_{\rm gr}(|\mathbf{r}_s - \mathbf{r}_i|)| \, \frac{\mathbf{r}_s - \mathbf{r}_i}{|\mathbf{r_s} - \mathbf{r}_i|}, \tag{6}$$

where $\mathbf{r}_s$ is the position of the skyrmion and $\mathbf{r}_i$ are the positions of the centers of the different grains.

To set the value of ΔK (needed for evaluating f_G) we follow the same procedure as in the Voronoi tessellation models:[30] we assume that the distribution of the values of the uniaxial anisotropy constant of the grains follows a normal distribution with mean value K and standard deviation σ_K. The value of ΔK is given to each grain randomly following the aforementioned normal distribution. Since $\mathbf{F}_G$ is randomly generated, for each set of parameters several simulations with different $\mathbf{F}_G$ are generated and averaged to get statistically significant results.

Equation (1) is a stochastic equation whose dependent variable is the position $\mathbf{r}_s$ of the skyrmion. Its corresponding Fokker-Planck equation can be derived (in a similar way as described in Ref. [29]):

$$\frac{\partial}{\partial t} p(\mathbf{r}, t) = -\nabla \cdot [p(\mathbf{r}, t)(\mathbf{v}_{\rm drv} + \mathbf{v}_{\rm ext})] + D_d \nabla^2 p(\mathbf{r}, t), \tag{7}$$

with the definitions

$$D_d = \frac{\gamma M_s^3 \alpha D k_B T}{\mu_0 (G^2 + D^2 \alpha^2 M_s^2)}, \tag{8}$$

$$\mathbf{v}_{\rm drv} = -M_s (\mathbb{G} - \alpha M_s \mathbb{D})^{-1} \mathbb{N} \mathbf{v}_H, \tag{9}$$

$$\mathbf{v}_{\rm ext} = -\gamma M_s^2 (\mathbb{G} - \alpha M_s \mathbb{D})^{-1} (\mathbf{F}_G + \mathbf{F}_R). \tag{10}$$

Equation (7) is a deterministic equation whose solution is $p(\mathbf{r}, t)$, the probability density of finding the center-of-mass of the skyrmion at position $\mathbf{r} = (x, y)$ at time t. It is a convection-

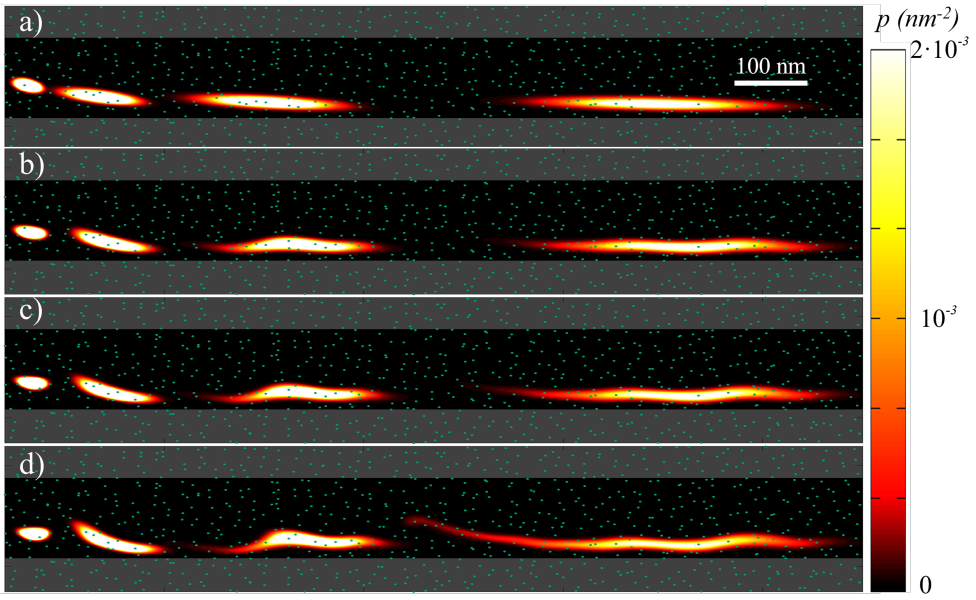

Figure 2: Overlapped snapshots of the probability density n of the presence of a skyrmion at a given position along the track for different times (1.7, 4.2, 6.7, and 11.7 ns). The distribution of the grains is the same in all figures but σ_K changes: σ_K=0(a), 0.05K(b), 0.1K (c), 0.2K(d). The side of the grains is $L_g = 20$ nm. The dots indicate the grain centers. The gray region indicates that skyrmion has reached the border and, thus, disappeared.

diffusion equation. The first term in the right-hand side indicates that the probability density is transported at a velocity $\mathbf{v}_{\rm drv} + \mathbf{v}_{\rm ext}$, whereas the second term is a linear, homogeneous, and isotropic diffusion term with constant D_d. Note that each of the solutions of the FPE [Eq. (7)] corresponds to infinitely many solutions of the STE [Eq. (1)] with the same grain distribution. To achieve the same accuracy as obtained by solving the FPE, the calculation time needed using the STE would be prohibitive.

Consider a skyrmion, initially at the position $(x_s, y_s) = (0, 0)$, traveling along the race-track while driven by a $\mathbf{v}_H = (0, -v_H)$. Our purpose is to study how the granularity of the sample, characterized by L_g and σ_K, affects the skyrmion dynamics at room temperature. To fix numbers, we use $\mathbf{v}_H = (0, -426.8)$ m s^{-1} and $f_0 = 8.71 \cdot 10^{-14}$ m^2 A^{-1}. These parameters are chosen so that, in the clean sample and at $T = 0$ K, the skyrmion travels at about 35 m s^{-1} when far from any border, speeding up to about 100 m s^{-1} when reaching the borders. The probability of surviving along the track a distance of 1.2 μm is found to be higher than

0.99998. The rest of the parameters used in the simulations are $\alpha = 0.3$, $M_s = 580$ kA m^{-1}, $K = 0.425$ MJ m^{-3}, $R = 80$ nm, $T = 300$ K, $W = 150$ nm, and $L = 1.2\,\mu$m.

In Fig. 2 we show four simulations considering the same grain distribution, but with different dispersion in the ΔK value, from $\sigma_K = 0$ (no granularity) to $\sigma_K = 0.2K$. Each plot shows a superposition of four snapshots (at different times) corresponding to the probability density of finding the skyrmion. In this way, the translation and the diffusion effect are clearly visualized. In particular, as σ_K becomes larger, skyrmions can be trapped or delayed more easily at some grains, stretching the probability density cloud. As a result, the probability of a skyrmion reaching a given distance along the track for a given time is expected to be reduced due to this grain-induced delay effect. In addition, even for infinite times, the probability of a skyrmion reaching a given position is reduced due to the pinning at some grains.

To quantify these results more accurately, the probability that a skyrmion reaches the position x of the track before a time t, or the skyrmion success probability, is calculated as

$$P_s(x,t) = \int_{-W}^{W} \mathrm{d}y' \int_0^t \mathrm{d}t'\, \hat{\mathbf{x}} \cdot \mathbf{J}_p(x,y',t'), \tag{11}$$

where $\mathbf{J}_p(x,y,t)$ is the probability current density. It can be obtained by considering that $\partial p(\mathbf{r},t)/\partial t = -\nabla \mathbf{J}_p$. After Eq. (7),

$$\mathbf{J}_p = (\mathbf{v}_{\mathrm{drv}} + \mathbf{v}_{\mathrm{ext}})p(\mathbf{r},t) - D_d\,\nabla p(\mathbf{r},t). \tag{12}$$

To have the potential to become a real device, the skyrmionic racetrack should ideally achieve a $P_s(L,\tau) = 1$ for reasonable times τ to be determined by the particular device in mind. This is because in general, one does not desire the skyrmions carrying information to "disappear", nor to reach their destination beyond the expected time.

In Fig. 3 we show the skyrmion success probability as it travels along the track for different σ_K. These results have been obtained after averaging the results of 30 simulations

[solutions of Eq. (7)] considering different distributions of grains with the same size $L_g = 20$ nm and σ_K.

In general, finding a skyrmion at a given distance and time is less likely for more heterogeneous samples (larger σ_K) indicating that the granularity somewhat delays the skyrmion. As time goes, the probability of reaching a given distance increases (naturally). After 100 ns (well after the longest time shown in the figures 3 and 4) we have observed that for the $\sigma_K = 0.2K$ case (red line in Fig. 3), the probability of reaching the 1.2 μm is about 0.85, indicating that the skyrmion has been lost, pinned, or greatly delayed.

There is a curious effect for small times. As seen in Fig. 3a the distances at which a skyrmion can be found is *larger* for more heterogeneous samples (the red line overcomes the other ones at $x \simeq 0.6\,\mu$m). This is because, when far from the edges, there is a substantial diffusion along the y axis and the cloud of probability density stretches significantly along y. When the skyrmion reaches the border, it is accelerated along x. Thus, the part of the $p(\mathbf{r}, t)$ cloud near the edge is then stretched along x. As a result, there is some relatively large probability of finding skyrmions in more heterogeneous samples at larger distances along x, with respect considering a plain sample. At larger times, this effect disappears since the $p(\mathbf{r}, t)$ distribution is already mostly concentrated near the borders in all cases.

We also studied how the defect size affects the performance of this device. In Fig. 4 we compare the results already shown in Fig. 3 for $\sigma_K = 0.1K$ and $0.2K$ with those using a different grain size, $L_g = 10$ nm. It is observed that the smaller the grains are, the weaker their effect is. This is because, when the grains are small, the skyrmions are much larger than them and, they seldom perceive the granularity. Actually, from the skyrmion perspective, it moves over an effectively uniform film. This is clearly seen in Fig. 4 where the small-grain results (dashed lines) practically match with the plain sample calculation (green solid line). In this case, if σ_K where very high, there could be some grain acting basically as a local point defect.[38] If the grains are much larger than the skyrmions then one would expect that the grain boundaries act as extended defects.[33]

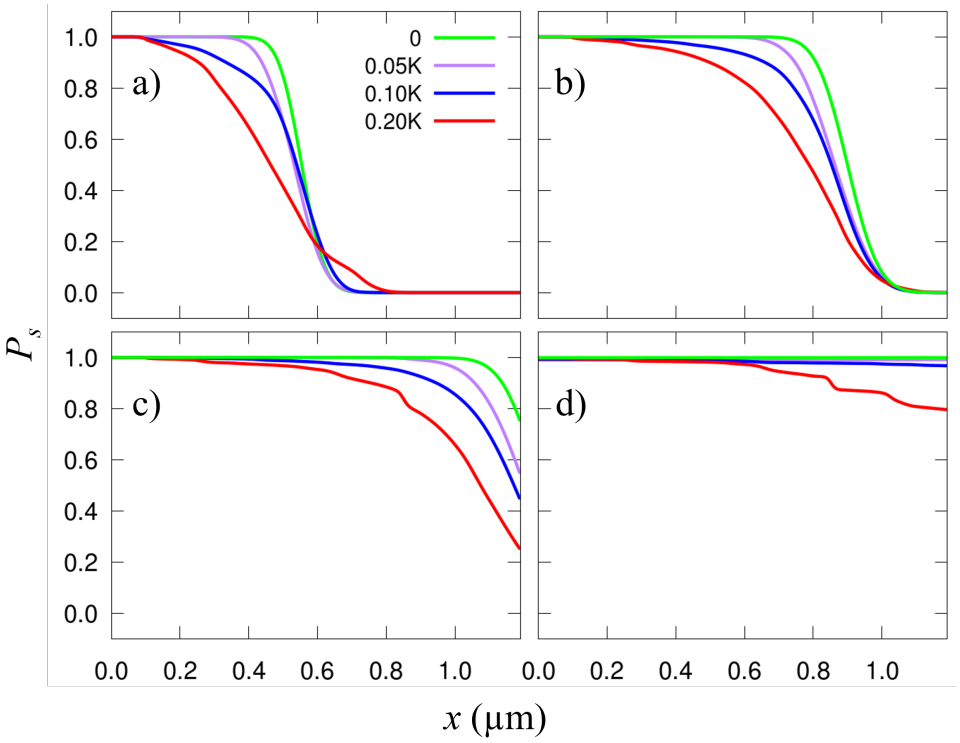

Figure 3: Probability of finding a skyrmion along a racetrack as a function of x. Each plot corresponds to a different time, from (a) to (d): t =6.67, 10, 13.33, and 20 ns. The different lines correspond to averaging 30 different grain distributions of side $L_g = 20$ nm with the same σ_K. $\sigma_K/K = 0$ (green), 0.05 (purple), 0.1 (blue), and 0.2(red).

Here, we have only took into account the anisotropy variations. In a strongly granular sample, other parameter changes may have to be taken into account as well. From our results we can conclude that trying to obtain more homogeneous racetracks is more important than obtaining monocrystalline racetracks, in terms of transport efficiency. In this sense, a sample with small grains (relative to the skyrmion size) acts as an effective homogeneous sample.

Of course, stronger variations of anisotropy, softer edge barriers, or other defects could yield in skyrmion loss. We have studied just a few particular cases because our goal was to study the effect of granularity. The main conclusion is that the information transport is not necessarily compromised due to the granularity (except for very heterogeneous samples), although the delay effect could be significant and, thus, a precise tracking of skyrmions and time synchronization of the readout would be necessary. For example, in a skyrmionic race-

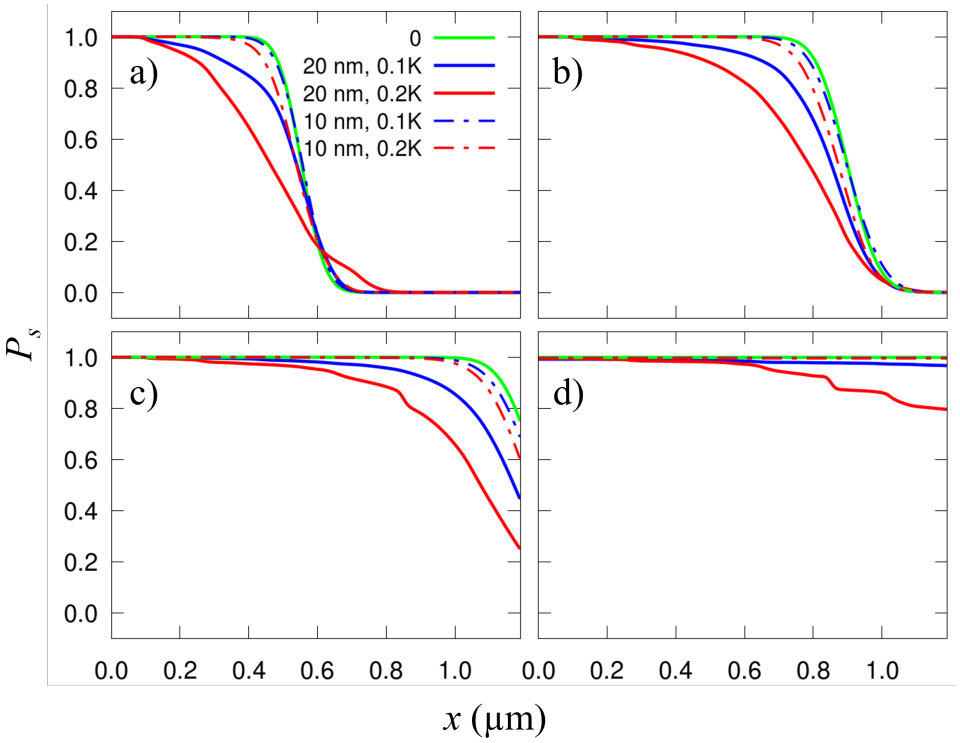

Figure 4: Probability of finding a skyrmion along a racetrack as a function of x. Each plot corresponds to a different time, from (a) to (d): t =6.67, 10, 13.33, and 20 ns. Solid blue and red curves are the same as in Fig. 3. The dotted curves of each color correspond to the respective σ_K but with smaller grains, $L_g = 10$nm. The green solid lines correspond to the clean racetrack and are included for comparison.

track memory, a chain of bits is a chain of skyrmions (1) and spaces without skyrmions (0). Hence, preserving the distance between skyrmions is mandatory for the proper functioning of the device. In this sense, racetracks require some kind of "synchronization points" for skyrmions. A possible solution could be considering wedges at the borders.[39] The overall velocity would be reduced, but the feasibility would be ensured.

The methodology presented here can be useful for controlling and somewhat harnessing the randomness in magnetic systems.[40] The "as realistic as possible" simulations are key ingredients in the design and development of a particular application. Neuromorphic computing systems,[41] logic and probabilistic computing devices,[42] or true random number generators[43] can benefit from the presented results and model.

We acknowledge Catalan project 2017-SGR-105 and Spanish project PID2019-104670GB-

I00 of Agencia Estatal de Investigación / Fondo Europeo de Desarrollo Regional (UE) for financial support. J. C.-Q. acknowledges a grant (FPU17/01970) from Ministerio de Ciencia, Innovación y Universidades (Spanish Government).

References

(1) Everschor-Sitte, K.; Masell, J.; Reeve, R. M.; Kläui, M. Perspective: Magnetic skyrmions—Overview of recent progress in an active research field. *Journal of Applied Physics* **2018**, *124*, 240901.

(2) Fert, A.; Cros, V.; Sampaio, J. Skyrmions on the track. *Nature Nanotechnology* **2013**, *8*, 152–6.

(3) Bourianoff, G.; Pinna, D.; Sitte, M.; Everschor-Sitte, K. Potential implementation of reservoir computing models based on magnetic skyrmions. *AIP Advances* **2018**, *8*, 055602.

(4) Wiesendanger, R. Nanoscale magnetic skyrmions in metallic films and multilayers: a new twist for spintronics. *Nature Reviews Materials* **2016**, *1*, 16044.

(5) Fert, A.; Reyren, N.; Cros, V. Magnetic skyrmions: advances in physics and potential applications. *Nature Reviews Materials* **2017**, *2*, 17031.

(6) Zhang, X.; Zhou, Y.; Ezawa, M.; Zhao, G. P.; Zhao, W. Magnetic skyrmion transistor: skyrmion motion in a voltage-gated nanotrack. *Scientific reports* **2015**, *5*, 11369.

(7) Hervé, M.; Dupé, B.; Lopes, R.; Böttcher, M.; Martins, M. D.; Balashov, T.; Gerhard, L.; Sinova, J.; Wulfhekel, W. Stabilizing spin spirals and isolated skyrmions at low magnetic field exploiting vanishing magnetic anisotropy. *Nature Communications* **2018**, *9*, 1015.

(8) Heinze, S.; von Bergmann, K.; Menzel, M.; Brede, J.; Kubetzka, A.; Wiesendanger, R.; Bihlmayer, G.; Blügel, S. Spontaneous atomic-scale magnetic skyrmion lattice in two dimensions. *Nature Physics* **2011**, *7*, 713–718.

(9) Boulle, O. et al. Room-temperature chiral magnetic skyrmions in ultrathin magnetic nanostructures. *Nature Nanotechnology* **2016**, *11*, 449–454.

(10) Sonntag, A.; Hermenau, J.; Krause, S.; Wiesendanger, R. Thermal stability of an interface-stabilized skyrmion lattice. *Physical Review Letters* **2014**, *113*, 077202.

(11) Moreau-Luchaire, C. et al. Additive interfacial chiral interaction in multilayers for stabilization of small individual skyrmions at room temperature. *Nature Nanotechnology* **2016**, *11*, 444–448.

(12) Soumyanarayanan, A.; Reyren, N.; Fert, A.; Panagopoulos, C. Emergent phenomena induced by spin–orbit coupling at surfaces and interfaces. *Nature* **2016**, *539*, 509–517.

(13) Woo, S. et al. Observation of room-temperature magnetic skyrmions and their current-driven dynamics in ultrathin metallic ferromagnets. *Nature Materials* **2016**, *15*, 501–506.

(14) Sampaio, J.; Cros, V.; Rohart, S.; Thiaville, A.; Fert, A. Nucleation, stability and current-induced motion of isolated magnetic skyrmions in nanostructures. *Nature Nanotechnology* **2013**, *8*, 839–844.

(15) Navau, C.; Del-Valle, N.; Sanchez, A. Analytical trajectories of skyrmions in confined geometries: Skyrmionic racetracks and nano-oscillators. *Physical Review B* **2016**, *94*, 184104.

(16) Bessarab, P. F.; Müller, G. P.; Lobanov, I. S.; Rybakov, F. N.; Kiselev, N. S.; Jónsson, H.; Uzdin, V. M.; Blügel, S.; Bergqvist, L.; Delin, A. Lifetime of racetrack skyrmions. *Scientific Reports* **2018**, *8*, 3433.

(17) Iwasaki, J.; Koshibae, W.; Nagaosa, N. Colossal Spin Transfer Torque Effect on Skyrmion along the Edge. *Nano Letters* **2014**, *14*, 4432–4437.

(18) Castell-Queralt, J.; González-Gómez, L.; Del-Valle, N.; Sanchez, A.; Navau, C. Accelerating, guiding, and compressing skyrmions by defect rails. *Nanoscale* **2019**, *11*, 12589–12594.

(19) Schulz, T.; Ritz, R.; Bauer, A.; Halder, M.; Wagner, M.; Franz, C.; Pfleiderer, C.; Everschor, K.; Garst, M.; Rosch, A. Emergent electrodynamics of skyrmions in a chiral magnet. *Nature Physics* **2012**, *8*, 301–304.

(20) Litzius, K. et al. Skyrmion Hall effect revealed by direct time-resolved X-ray microscopy. *Nature Physics* **2016**, *13*, 170–175.

(21) Salimath, A.; Abbout, A.; Brataas, A.; Manchon, A. Current-driven skyrmion depinning in magnetic granular films. *Physical Review B* **2019**, *99*, 104416.

(22) Raposo, V.; Luis Martinez, R. F.; Martinez, E. Current-driven skyrmion motion along disordered magnetic tracks. *AIP Advances* **2017**, *7*, 056017.

(23) Kim, J.-V.; Yoo, M.-W. Current-driven skyrmion dynamics in disordered films. *Applied Physics Letters* **2017**, *110*, 132404.

(24) Legrand, W.; Maccariello, D.; Reyren, N.; Garcia, K.; Moutafis, C.; Moreau-Luchaire, C.; Collin, S.; Bouzehouane, K.; Cros, V.; Fert, A. Room-Temperature Current-Induced Generation and Motion of sub-100 nm Skyrmions. *Nano Letters* **2017**, *17*, 2703–2712.

(25) Miltat, J.; Rohart, S.; Thiaville, A. Brownian motion of magnetic domain walls and skyrmions, and their diffusion constants. *Physical Review B* **2018**, *97*, 214426.

(26) Troncoso, R. E.; Núñez, A. S. Thermally assisted current-driven skyrmion motion. *Physical Review B* **2014**, *89*, 224403.

(27) Zhao, L.; Wang, Z.; Zhang, X.; Liang, X.; Xia, J.; Wu, K.; Zhou, H.-A.; Dong, Y.; Yu, G.; Wang, K. L.; Liu, X.; Zhou, Y.; Jiang, W. Topology-Dependent Brownian Gyromotion of a Single Skyrmion. *Phys. Rev. Lett.* **2020**, *125*, 027206.

(28) Zhang, X.; Ezawa, M.; Zhou, Y. Thermally stable magnetic skyrmions in multilayer synthetic antiferromagnetic racetracks. *Physical Review B* **2016**, *94*, 064406.

(29) Castell-Queralt, J.; González-Gómez, L.; Del-Valle, N.; Navau, C. Deterministic approach to skyrmionic dynamics at nonzero temperatures: Pinning sites and racetracks. *Phys. Rev. B* **2020**, *101*, 140404.

(30) Del-Valle, N.; Castell-Queralt, J.; González-Gómez, L.; Navau, C. Defect modeling in skyrmionic ferromagnetic systems. *APL Materials* **2022**, *10*, 010702.

(31) Thiele, A. Steady-State Motion of Magnetic Domains. *Physical Review Letters* **1973**, *30*, 230–233.

(32) Liu, L.; Lee, O. J.; Gudmundsen, T. J.; Ralph, D. C.; Buhrman, R. A. Current-Induced Switching of Perpendicularly Magnetized Magnetic Layers Using Spin Torque from the Spin Hall Effect. *Physical Review Letters* **2012**, *109*, 096602.

(33) González-Gómez, L.; Castell-Queralt, J.; Del-Valle, N.; Sanchez, A.; Navau, C. Analytical modeling of the interaction between skyrmions and extended defects. *Physical Review B* **2019**, *100*, 054440.

(34) Zhang, X.; Müller, J.; Xia, J.; Garst, M.; Liu, X.; Zhou, Y. Motion of skyrmions in nanowires driven by magnonic momentum-transfer forces. *New Journal of Physics* **2017**, *19*, 065001.

(35) Garcia-Sanchez, F.; Sampaio, J.; Reyren, N.; Cros, V.; Kim, J.-V. A skyrmion-based spin-torque nano-oscillator. *New Journal of Physics* **2016**, *18*, 075011.

(36) Lau, J. W.; Memichael, R. D.; Donahue, M. J. Implementation of Two-Dimensional Polycrystalline Grains in Object Oriented Micromagnetic Framework. *Journal of Research of the National Institute of Standards and Technology* **2009**, *114*, 57.

(37) Gong, X.; Yuan, H. Y.; Wang, X. R. Current-driven skyrmion motion in granular films. *Phys. Rev. B* **2020**, *101*, 064421.

(38) Navau, C.; Del-Valle, N.; Sanchez, A. Interaction of isolated skyrmions with point and linear defects. *Journal of Magnetism and Magnetic Materials* **2018**, *465*, 709–715.

(39) Morshed, M. G.; Vakili, H.; Ghosh, A. W. Positional Stability of Skyrmions in a Racetrack Memory with Notched Geometry. *Phys. Rev. Applied* **2022**, *17*, 064019.

(40) Navau, C.; Sort, J. Exploiting random phenomena in magnetic materials for data security, logics, and neuromorphic computing: Challenges and prospects. *APL Materials* **2021**, *9*, 070903.

(41) Song, K. M. et al. Skyrmion-based artificial synapses for neuromorphic computing. *Nature Electronics 2020 3:3* **2020**, *3*, 148–155.

(42) Zázvorka, J.; Jakobs, F.; Heinze, D.; Keil, N.; Kromin, S.; Jaiswal, S.; Litzius, K.; Jakob, G.; Virnau, P.; Pinna, D.; Everschor-Sitte, K.; Rózsa, L.; Donges, A.; Nowak, U.; Kläui, M. Thermal skyrmion diffusion used in a reshuffler device. *Nature Nanotechnology 2019 14:7* **2019**, *14*, 658–661.

(43) Medlej, I.; Hamadeh, A.; Hassan, F. E. H. Skyrmion based random bit generator. *Physica B: Condensed Matter* **2020**, *579*, 411900.